INTERNATIONAL JOURNAL OF CLIMATOLOGY
Int. J. Climatol. (2011)
Published online in Wiley Online Library
(wileyonlinelibrary.com) DOI: 10.1002/joc.2364

RMetS
Royal Meteorological Society

GCM projections for the Pacific Decadal Oscillation under greenhouse forcing for the early 21st century

Suzan L. Lapp,* Jeannine-Marie St. Jacques,* Elaine M. Barrow and David J. Sauchyn
Prairie Adaptation Research Collaborative (P.A.R.C.), 2 Research Drive, University of Regina, Regina, SK, Canada

ABSTRACT: The climatology and hydrology of western North America display strong periodic cycles which are correlated with the low-frequency Pacific Decadal Oscillation (PDO). The PDO's signature is seen throughout the entire North Pacific region, with related significant associations to hydrology and ecology in western North America and northeastern Asia. Therefore, the status of the PDO in a warmer world caused by anthropogenic climate change is of great interest. We developed early 21st-century projections of the PDO, using data from archived runs of the most recent high-resolution global climate models from the Intergovernmental Panel on Climate Change (IPCC) Fourth Assessment Report (Phase 3 of the Coupled Model Intercomparison Project). Because of the geographical adjacency and hypothesized interactions between the PDO and the El Niño-Southern Oscillation (ENSO), and between the PDO and the North Atlantic Oscillation/Arctic Oscillation (NAO/AO), we also developed concurrent projections of ENSO and the NAO and examined their relationships with the projected PDO. For the B1, A1B and A2 Special Report on Emissions Scenarios (SRES) emission scenarios, the PDO projections for 2000–2050 showed a weak multi-model mean shift towards more occurrences of the negative phase PDO, which becomes statistically significant for the time period 2000–2099. However, not all the models showed a consistent shift to negative PDO conditions. Copyright © 2011 Royal Meteorological Society

KEY WORDS PDO; ENSO; NAO; AO; Global Climate Model projections; CMIP3

Received 29 April 2010; Revised 11 April 2011; Accepted 18 April 2011

1. Introduction

The Pacific Decadal Oscillation (PDO) is a re-occurring sea surface temperature (SST) pattern that describes a large amount of North Pacific Ocean variability (Mantua *et al*., 1997; Zhang *et al*., 1997; Mantua and Hare, 2002). When the PDO is in its warm or positive phase, SSTs in the central north Pacific are relatively low and northeastern Pacific SSTs are warmer and vice versa in the cool or negative phase. The low-frequency PDO shifts phases on an inter-decadal time scale, usually at about 20–35 years (Minobe, 1997, 1999; Mantua and Hare, 2002) from warm to cool phases in 1890 and 1947 and from cool to warm in 1925 and 1977 (Minobe, 1997; Deser *et al*., 2004). The PDO is primarily a wintertime (November to March) phenomenon.

The PDO has significant correlations with the climatology and hydrology of northwestern North America (Mantua *et al*., 1997; Mantua and Hare, 2002; McCabe and Dettinger, 2002; Stewart *et al*., 2005; St. Jacques *et al*., 2010; Whitfield *et al*., 2010; Wise, 2010). Winter precipitation in this region is higher (lower) and winter temperatures are cooler (warmer) when the PDO is in a negative (positive) phase, and vice versa in southwestern North America (Mantua *et al*., 1997; Mantua and Hare, 2002). Therefore, strong negative correlations exist between the PDO and precipitation and river discharge in the Pacific Northwest and corresponding positive correlations in the American southwest and northern Mexico. The PDO's signature is also seen throughout the North Pacific region, with related significant associations in Alaskan, northeastern Siberian, Manchurian, Korean and Japanese hydroclimatology (Mantua and Hare, 2002; Deser *et al*., 2004). Physical oceanographic patterns propagate into ecological impacts as strong fingerprints of the PDO are shown in ocean productivity and fisheries populations (Mantua *et al*., 1997; Francis *et al*., 1998; McGowan *et al*., 1998; Anderson and Piatt, 1999; Mantua and Hare, 2002; Zhang *et al*., 2004; Chen and Hare, 2006).

The precise nature of the couplings among the extratropical North Pacific Ocean and its overlying atmosphere is an active research area, with much evidence suggesting that the North Pacific atmospheric circulation actually drives the underlying mixed-layer oceanic variability (Davis, 1976; Trenberth and Hurrell, 1994; Lau, 1997; Kushnir *et al*., 2002). However, the PDO reflects an integrated or rectified measure of the North Pacific atmosphere-ocean system. Given this and the PDO's multiple, major linkages with the northern Pacific Basin's climatology, hydrology and marine ecology, its status in a warmer world caused by anthropogenic climate change is of great interest. In this study, we developed early 21st-century projections of the PDO, using data from

* Correspondence to: Suzan L. Lapp and Jeannine-Marie St. Jacques, Prairie Adaptation Research Collaborative (P.A.R.C.), 2 Research Drive, University of Regina, Regina, SK, Canada.
E-mail: lapp200s@uregina.ca; stjacqje@uregina.ca

archived runs of the most recent high-resolution global climate models (GCMs), and examined whether there was a clear tendency for the models to demonstrate a shift in the North Pacific Ocean towards more positive or negative PDO phase-like conditions. This study is the first to explicitly project the PDO as calculated by EOF analysis of North Pacific SST residuals, as defined by Mantua *et al*. (1997) and Zhang *et al*. (1997). Because of the hypothesized interactions between the PDO and the El Niño-Southern Oscillation (ENSO), and between the PDO and the North Atlantic Oscillation/Arctic Oscillation (NAO/AO), we also examined the concurrent projection of ENSO and the NAO.

2. PDO projection method

As a part of the Intergovernmental Panel on Climate Change (IPCC) Fourth Assessment Report (AR4) Phase 3 of the Coupled Model Intercomparison Project (CMIP3), international modelling centres submitted their projections for the 21st century under different emission scenarios, together with their simulations of 20th-century climate and control runs to scrutiny by the wider scientific community (Meehl *et al*., 2007). These data from 23 GCMs are archived by the Program for Climate Model Diagnosis and Intercomparison (PCMDI) of Lawrence Livermore National Laboratory (http://www-pcmdi.llnl.gov/ipcc/about_ipcc,php). Details of the GCMs are found in IPCC4 (2007), Table VIII.1. Because of the importance of recurring large-scale climate patterns (e.g. the PDO, ENSO) for regional climates, researchers have begun to critically examine these CMIP3 runs for their capacity to model atmosphere-ocean climate oscillations (Muller and Roeckner, 2006; IPCC4, 2007; Overland and Wang, 2007; Yu and Zwiers, 2007; Oshima and Tanimoto, 2009; Stoner *et al*., 2009; Wang *et al*., 2010). From the 23 GCMs with archived data, we chose those best able to simulate the PDO, using comparisons of spatial and temporal patterns of variability from the 20th-century observed records, the 20th-century simulations and the control runs. We specifically examined the GCMs' capacity to simulate low-frequency variability using the multi-century pre-industrial control runs, which were initially run to ensure model stability and determine the models' representation of natural climate variability. To project the PDO into the future, we selected model runs under the B1, A1B and A2 Special Report on Emissions Scenarios (SRES) emission scenarios, which were available for nearly all GCMs (Nakicenovic *et al*., 2000).

In order to project the PDO, a method of calculating the PDO must be selected from various algorithms available (Mantua *et al*., 1997; Minobe, 1997; Overland and Wang, 2007; Zhang *et al*., 1997; Oshima and Tanimoto, 2009). For the calculation of the PDO from instrumental data, we followed the method described in Mantua *et al*. (1997) (ftp://ftp.atmos.washington.edu/mantua/pdofiles/) and Zhang *et al*. (1997). Our PDO index is the leading Principal Component (PC) from an unrotated EOF analysis of monthly 'residual' North Pacific SST anomalies, poleward of 20°N for the 1900–1993 time period. 'Residuals' are the difference between the observed monthly SST anomalies and the monthly mean global average SST anomaly (Zhang *et al*., 1997). The PDO index post-1993 was calculated by projecting the 1994–2008 observed and 1994–2050 GCM residual SST anomalies onto the leading eigenvector or loading pattern (EOF 1) from the 1900 to 1993 SST data (Mantua, personal communication). All EOF analyses were performed with MATLAB©. Any further analyses using the PDO index were done with November to March averaged data, with the individual months first normalized by 1961–1990. Our main methodological divergence from Mantua *et al*. (1997) lies in our use of the later and more complete sea surface temperature HadSST2 data set (Rayner *et al*., 2003) (http://www.cru.uea.ac.uk/cru/data/temperature/), rather than the earlier HadSST1 (Folland and Parker, 1990, 1995) and the optimally interpolated SST data (Reynolds and Smith, 1995). Following are more detailed accounts of the derivation of the PDO index from observed and modelled SSTs.

2.1. Calculation of the PDO for 1900–2008 from observed SST data

Data used: monthly SST-centred anomalies from the HadSST2 data set for 1900–2008 (http://www.cru.uea.ac.uk/cru/data/temperature/).

The data are arranged as a $5^\circ \times 5^\circ$ grid covering the global ocean, with the first grid point centred at 177.5 °W and 87.5 °N. These SSTs are standardized at each grid point by subtracting the monthly means for 1961–1990 calculated from each individual grid point. The 2009 data were not yet available when this analysis was performed.

2.1.1. Method

(1) North_Pacific_SST_grid represents all grid points in the North Pacific Ocean north of 20°N and south of 65°N in the HadSST2 data set, consisting of 197 grid points in total. North_Pacific_SST defines the field of SST anomalies (from HadSST2) from the grid points in North_Pacific_SST_grid, covering 1900–2008. This field consists of 197 time series, each of length 1308 (12 months × 109 years).

(2) Global_Ocean_SST_grid represents all grid points in the global ocean north of 35 °S and south of 75°N in the HadSST2 data set. A large portion of the Southern Ocean is deleted because there simply are not enough SST data spanning 1900–2008 in this region. There are a total of 1177 grid points in this data set.

(3) Using the Global_Ocean_SST_grid locations, a monthly mean global SST anomaly time series (Observed_global_mean) was calculated for 1900–2008, i.e. for each month in each year, the mean SST anomaly was computed over the entire global ocean. The Observed_global_mean data set has a length of 1308 (12 months × 109 years).

(4) A Residual_observed_SST_anomaly field for the North Pacific was created by subtracting, component-wise, the Observed_global_mean time series from

each individual SST time series in North_Pacific_SST_grid.

(5) The Residual_observed_SST_anomaly field was truncated to consist of data only from 1900–1993, with the resulting field called 1900–1993_Residual_observed_SST_anomaly. The data from each of the 197 grid locations are now time series of length 1128 (12 months × 94 years). An EOF analysis of the 1900–1993_Residual_observed_SST_anomaly field was undertaken using the temporal covariance matrix, without any normalization or rotation (Bjornsson and Venegas, 1997; Wilks, 2006). In performing the EOF analysis, missing data points were set to zero. Owing to the paucity of data from the North Pacific in the earlier decades of the 1900s, this was an issue that had to be addressed. The PDO index for 1900–1993 is the leading PC time series (or PC 1) from this analysis. Mapping the leading eigenvector or loading pattern produces the 1900–1993 PDO pattern in the North Pacific (Figure 1).

(6) PDO index values for 1994–2008 were computed differently, following the methodology of Mantua *et al*. (1997). The Residual_observed_SST_anomaly field was truncated to consist of data only from 1994–2008, with this field being called 1994–2008_Residual_observed_SST_anomaly. The data from each of the 197 grid locations are now time series of length 192 (12 months × 16 years). Projecting the 1994–2008_Residual_observed_SST_anomaly field onto the leading eigenvector from step (5) gives the PDO index for 1994–2008.

(7) The monthly PC time series was normalized relative to 1961–1990 (i.e. centred by subtracting the corresponding monthly mean for 1961–1990 and then divided by the corresponding standard deviation) and winter (November to March) indices were extracted and then averaged together.

2.2. Calculation of the PDO for 1900–2050 from GCM data

This was computed analogously to above, simply replacing the observed SST data by GCM SST data. For each chosen GCM and for each of its archived paired 20th and 21st-century runs, the GCM SSTs were regridded, using MATLAB©, to the same $5^\circ \times 5^\circ$ gridcell size as the Hadley Centre SST data set for direct comparison.

We started with the 12 CMIP3 models that Wang *et al*. (2010) deemed suitable for projecting the PDO (using only those which had full 20th-century simulation runs available). Wang *et al*. (2010) and Overland and Wang (2007) used a simpler method based upon EOF analysis of SSTs in their seminal papers, rather than EOF analysis of the residual SSTs, as Mantua *et al*. (1997) and Zhang *et al*. (1997) defined the PDO to be. First, in order to determine the GCMs best able to simulate the observed PDO spatial pattern, we compared, via spatial correlation coefficients, the mapped leading eigenvector (EOF 1) from an unrotated EOF residual analysis of each 20th-century simulation run to the mapped EOF 1 of the observed North Pacific residual data ('the PDO pattern'). Only GCMs with correlations greater than 0.7 with the observed North Pacific EOF 1 were considered suitable for further analysis.

Because of the geographical adjacency and the hypothesized interactions between the PDO and ENSO and between the PDO and the NAO/AO, we decided that any GCM used for PDO projection must also reasonably reproduce a recognizable ENSO and NAO/AO. This manuscript takes no part in the debate about whether or not the NAO is a manifestation of the AO, but simply uses the close relationship between the two indices that allows the NAO to be a proxy for the AO. We used the averaged June to November Southern Oscillation Index (SOI) [i.e. the normalized difference between monthly mean sea level pressure (SLP) at Tahiti and Darwin] as our ENSO metric (Ropelewski and Jones, 1987) and the difference between winter (December to March) monthly normalized mean SLP at Gibraltar and Reykjavik as our NAO metric (Jones *et al*., 1997). We use the two-point SLP definitions of the SOI and NAO, with their centennial length time series, given our focus on the low-frequency variability of the PDO. We visually compared the correlation map of the observed SOI with Pacific SLPs to similar correlation maps of the SOI for each 20th-century simulation run. Likewise, we compared the correlation map of the observed NAO with northern hemisphere Atlantic-centred SLPs to similar correlation maps of the NAO for each 20th-century simulation run. Only GCMs which produced a recognizable SOI and NAO spatial pattern were analysed further.

The statistical significance of changes in the PDO, SOI and NAO indices between 1900–1999 and 2000–2050 were assessed by two-tailed t-tests, for each individual run and the multi-model mean, comparing the simulation mean index for each emissions scenario to the corresponding projected mean index. Autocorrelation was present in many of the time series. Hence, the significance of any shift in the mean of an index was assessed using a Monte Carlo t-test (Manly, 1998). Using the R programming language Version 2.9.1 the full 150-year index was randomly shuffled and divided into a 99-year initial portion and a 51-year latter portion and a t-statistic between the two was computed (R Development Core Team, 2008). This was done 10 000 times. The number of times the actual t-statistic exceeded the randomly simulated t-statistic was determined, as well as the number of times the converse occurred, and the two-tailed significance was assessed at the 5% level.

In order to ascertain if the observed PDO was still present in the same form in the projected 2000–2050 North Pacific Ocean, we performed a similar unrotated EOF analysis of the 2000–2050 residual projected SST anomalies. The mapped EOF 1 and EOF 2 were then compared by spatial correlation to EOF 1 and EOF 2 from the 1900 to 1993 observed data. We then undertook two further analyses to determine how similar the GCM-derived PDO indices were to the observed

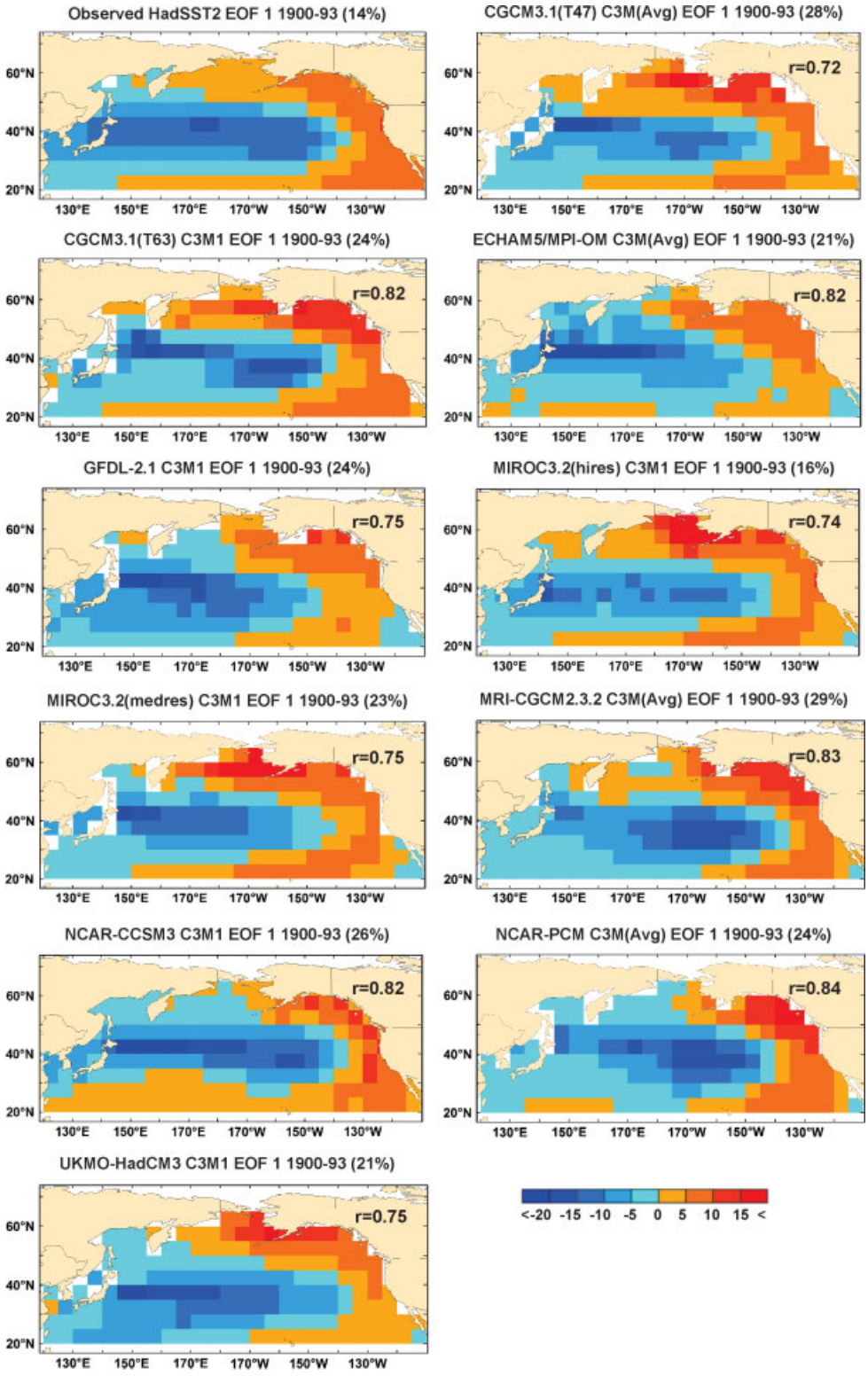

Figure 1. The spatial patterns of the leading EOFs of North Pacific SST residuals for the ten chosen CMIP3 models, based upon the 20th-century simulations, together with that from the PDO (i.e. EOF 1 from the observed 1900–1993 HadSST2 data). The percent variance explained is given after the model name; spatial correlation coefficients from comparison with the 1900–1993 observed PDO pattern indicated in the upper right hand corner. Colour scale shows PCA loadings (×100). If multiple runs were available for a model, ensemble means are presented for brevity. This figure is available in colour online at wileyonlinelibrary.com/journal/joc

PDO. First, we examined the GCMs for their capacity to produce the low-frequency variability at periodicities characteristic of the PDO, i.e approximately 20 and 60 years (Minobe, 1997, 1999; Chao *et al.*, 2000). We calculated a pre-industrial PDO by projecting the pre-industrial residual SSTs from the control runs onto the GCMs' 1900–1993 EOF 1. Using multi-taper method spectral analysis (MTM), the pre-industrial PDO indices

Table I. List of chosen coupled atmosphere-ocean models which archived the required fields, their details, number of available 21st-century runs per scenario, and length of the pre-industrial control runs (run 1 used).

GCM No.	IPCC4 GCM ID	Country	Atmosphere resolution	Ocean resolution	Number 21st-century runs			Control run length (years)
					B1	A1B	A2	
1	**CGCM3.1(T47)**	Canada	3.7° × 3.7° L31	1.84° × 1.85° L29	3	3	3	500
2	**CGCM3.1(T63)**	Canada	2.8° × 2.8° L31	1.4° × 0.9° L29	1	1	0	400
3	**ECHAM5/MPI-OM**	Germany	1.875° × 1.865° L31	1.5° × 1.5° L40	2	2	1	na
4	**GDFL-CM2.1**	USA	2.5° × 2.0° L24	1.0° × 1.0° L50	1	1	1	501
5	**MIROC3.2(hires)**	Japan	1.125° × 1.12° L56	0.28° × 0.188° L47	1	0	1	100
6	**MIROC3.2(medres)**	Japan	2.8° × 2.8° L20	(0.5–1.4°) × 1.4° L43	1	1	1	500
7	**MRI-CGCM2.3.2**	Japan	2.8° × 2.8° L31	(0.5–2.5°) × 2.0° L23	5	5	5	350
8	**NCAR-CCSM3**	USA	1.4° × 1.4° L26	(0.3–1.0°) × 1.0° L40	1	0	1	500
9	**NCAR-PCM**	USA	2.8° × 2.8° L18	(0.5–0.7°) × 0.7° L32	2	2	2	na
10	**UKMO-HadCM3**	UK	3.75° × 2.5° L15	1.25° × 1.25° L20	1	1	1	340

"na" means no run was archived.

were then examined for similar temporal variability as the observed PDO index. Adaptively weighted spectra with a red noise background were used (five tapers) (Mann and Lees, 1996) (SSA-MTM Toolkit for spectral analysis, http://www.atmos.ucla.edu/tcd/ssa/). Additionally, the PDO indices derived from the 20th-century simulation runs were examined with MTM (three tapers used with these shorter records).

Second, in order to examine if the chosen GCMs replicate the observed 20th-century temporal coherence between the PDO and ENSO (Kiem *et al*., 2003; Verdon and Franks, 2006; Stahl *et al*., 2006), we compared frequencies of co-occurring strong in-phase positive (negative) PDO events and strong or moderate El Niño (La Niña) events and the out-of-phase events [i.e. strong positive (negative) PDO events and strong or moderate La Niña (El Niño)]. Strong or moderate El Niño events were defined as when the averaged June to November SOI was <-0.5 and a La Niña event was when the averaged June to November SOI was >0.5, following Redmond and Koch (1991). These authors found better correlations between the SOI and winter climate when the SOI leads by a few months; therefore we maintained this relationship by comparing the leading SOI (June to November) event to the following PDO event (November to March). Only strong PDO events, where the absolute magnitude of the PDO was ≥ 0.7 standard deviations (Bond and Harrison, 2000), were used in this analysis (analysis using 0.5 standard deviations gave similar results). Chi-square tests were used to determine if the frequencies of the in-phase positive PDO/El Niño and negative PDO/La Niña occurrences and the out-of-phase positive PDO/La Niña and negative PDO/El Niño occurrences were the same in the 20th-century simulation runs for each chosen GCM as in the observed data for 1900–1999. As a further exploration of changes in North Pacific variability, chi-square tests were also used to determine if the frequencies of the in-phase PDO/ENSO occurrences and the out-of-phase PDO/ENSO occurrences were the same in the projected data for 2000–2050 as in the 20th-century simulated runs for each chosen GCM and emissions scenario.

3. Results

Our final set of GCMs was CGCM3.1 (T47) (Flato, 2005), CGCM3.1 (T63) (Flato, 2005), ECHAM5/MPI-OM (Roeckner *et al*., 2003), GDFL-CM2.1 (Delworth *et al*., 2006), MIROC3.2 (hires) (Hasumi and Emori, 2004), MIROC3.2 (medres) (Hasumi and Emori, 2004), MRI-CGCM2.3.2 (Yukimoto *et al*., 2001; Yukimoto and Noda, 2003), NCAR-CCSM3 (Collins *et al*., 2006), NCAR-PCM (Washington *et al*., 2000) and UKMO-HadCM3 (Gordon *et al*., 2000; Pope *et al*., 2000) (Table I). These ten chosen models reproduced the spatial pattern of the observed 20th-century PDO well (Figure 1). However, the simulated 20th-century PDOs typically explained more North Pacific residual variance in comparison to the actual observed variability, with the possible exception of MIROC (hires). All ten GCMs produced a recognizable 20th-century SOI and NAO index spatial pattern as shown by the comparison of correlation maps of the observed June to November SOI with Pacific SLPs, and the observed winter NAO with northern hemisphere SLPs to similar correlation maps of each 20th-century simulated SOI with SLPs and the simulated NAO with SLPs (Figures 2 and 3).

Two of Wang *et al*. (2010)'s models were dropped: ECHO-G and GDFL2.0, and CGCM3.1 (T47) runs 4 and 5. Our analysis required that SST and SLP output from each GCM be available for both the 20th century and 21st century in concurrent runs; often GCMs have several runs for the 20th century but with only one or two of these runs continuing through the 21st century for the different emission scenarios. Overland and Wang (2007) and Wang *et al*. (2010) considered the GFDL 2.0 model to produce acceptable PDO simulations both temporally and spatially; however, our results differ.

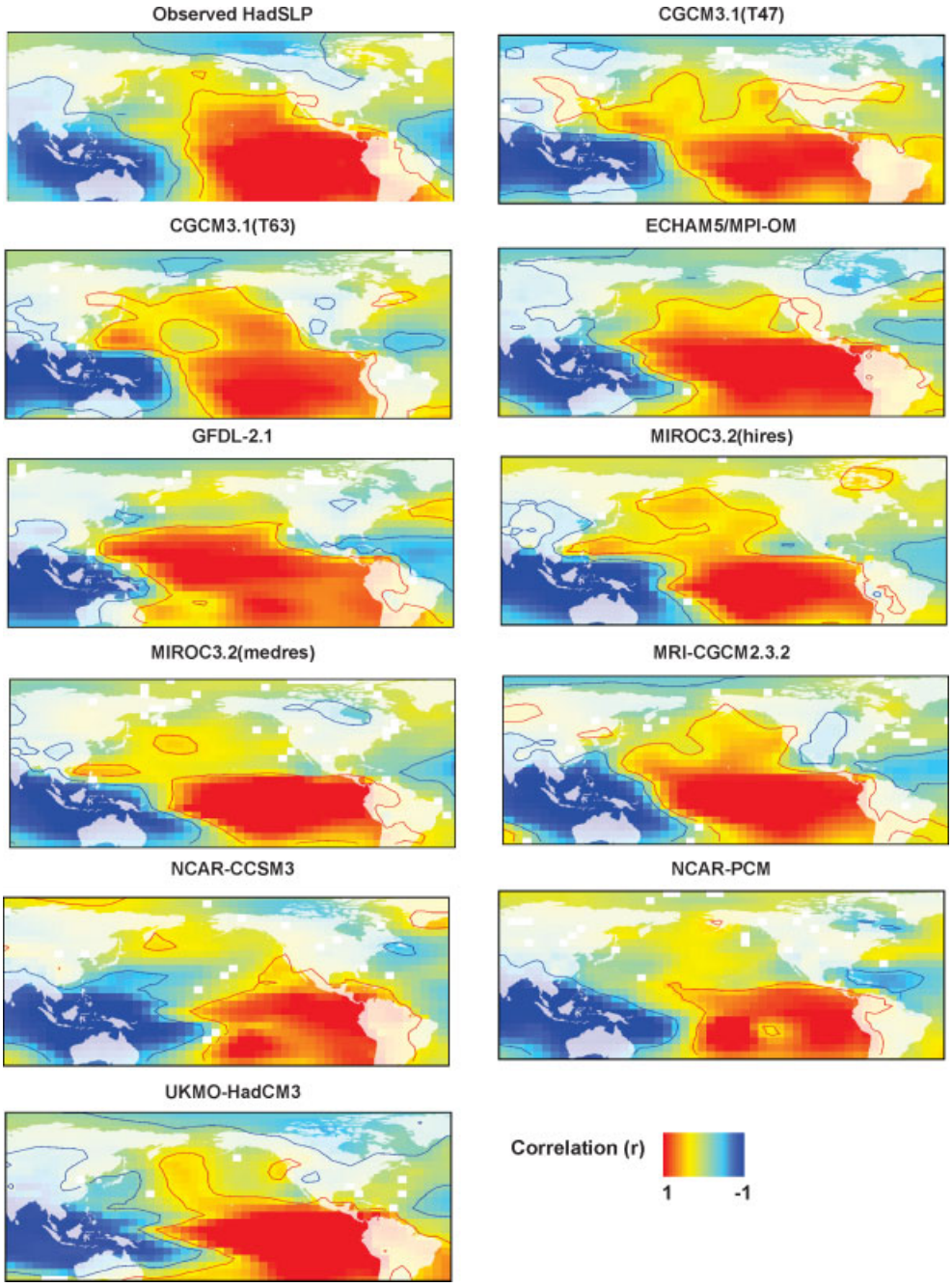

Figure 2. Pearson's correlation map of the observed June to November Southern Ocean Index (SOI) (Earth Systems Research Laboratory, http://www.cdc.noaa.gov/ClimateIndices/) with observed SLPs from the HadSLP1 data set (Met Office Hadley Centre, http://badc.nerc.ac.uk) for the 1900–1999 period, together with correlation maps of the simulated SOI for 1900–1999 with the simulated SLPs for each of the ten selected GCMs (refer to text). Thick red (blue) line denotes the positive (negative) correlation at the 95% significance level. This figure is available in colour online at wileyonlinelibrary.com/journal/joc

Overland and Wang (2007) compared the first EOF spatial pattern using the 20th-century simulation GCM ensemble mean (i.e. average of the runs) to the observed North Pacific EOF 1 spatial pattern, rather than each individual run as only one run continued through the 21st century. We conducted an EOF analysis on this GFDL 2.0 run for the 20th-century simulation and found that EOF 1 correlated with HadSST2 EOF2 and EOF 2 correlated with HadSST2 EOF 1; therefore we excluded this GCM from the analysis. We also dropped ECHO-G and CGCM3.1 (T47) runs 4 and 5 because their EOF 1's correlated with HadSST2 EOF 2 and their EOF 2's correlated with HadSST2 EOF 1.

Early 21st-century PDO projections showed a non-significant shift towards more negative phase PDO conditions for all three emissions scenarios (Figure 4, Tables II and III). This can be seen by comparing the multi-model 1900–1999 simulation means to the multi-model 2000–2050 means summarized in Table II (in computing

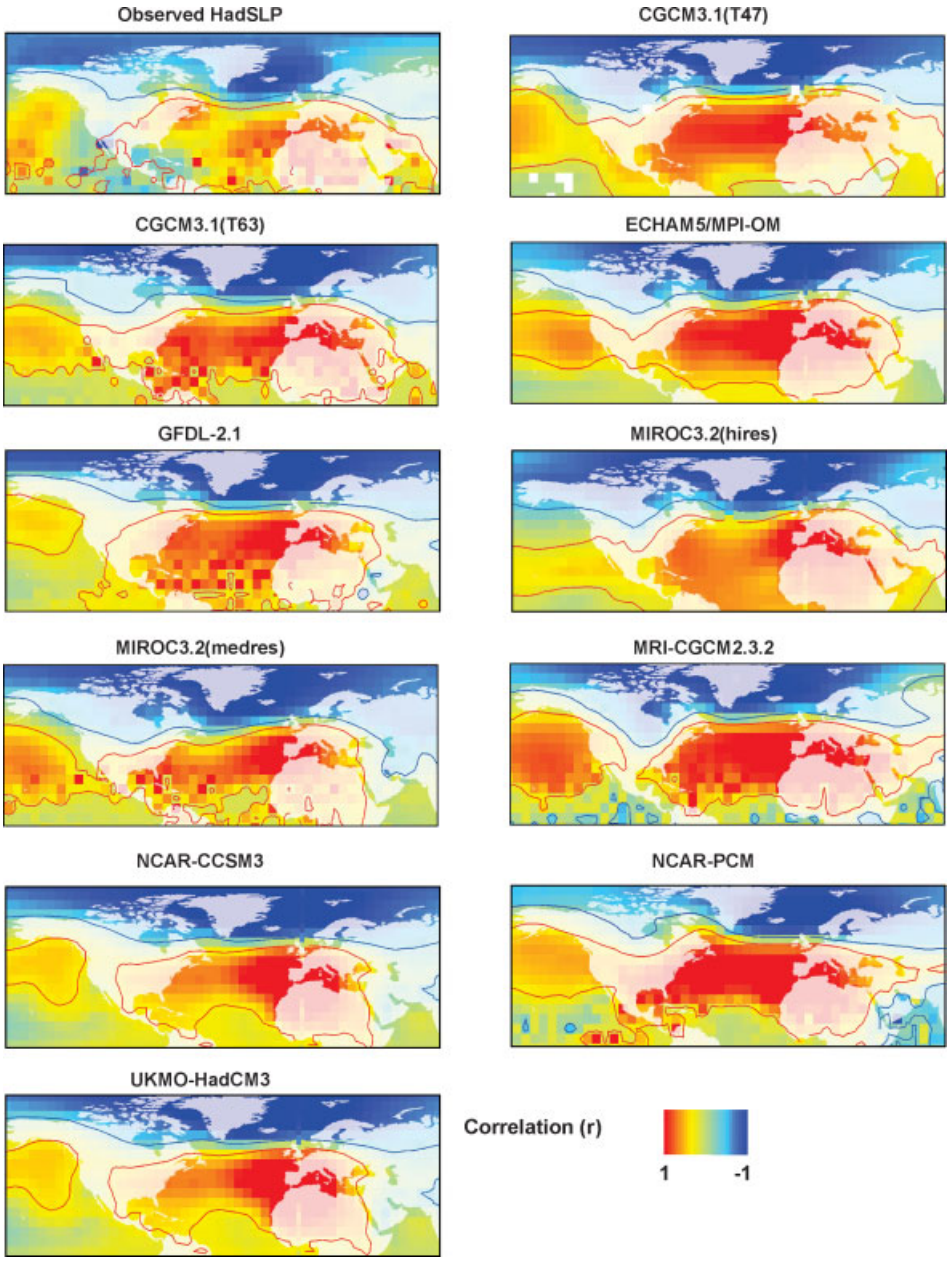

Figure 3. Pearson's correlation map of the observed winter NAO index (Earth Systems Research Laboratory, http://www.cdc.noaa.gov/ClimateIndices/) with observed SLPs from the HadSLP1 data set (Met Office Hadley Centre, http://badc.nerc.ac.uk) for the 1900–1999 period, together with correlation maps of the simulated NAO for 1900–1999 with the simulated SLPs for each of the ten selected GCMs (refer to text). Thick red (blue) line denotes the positive (negative) correlation at the 95% significance level. This figure is available in colour online at wileyonlinelibrary.com/journal/joc

the multi-model mean, all runs were weighted equally, following Knutti *et al*., 2010). Although in this study the emphasis is on projections for 2000–2050, projections were also computed for 2000–2099. For all three emissions scenarios, the 2000–2099 multi-model mean showed a significant (at the 10% level) shift towards the negative phase of the PDO (Table II). Comparison of the 1900–1999 simulation individual run means to the actual 1900–1999 observed mean PDO index showed that almost all the simulations produced more occurrences of negative phase PDO than were actually observed, except for CGCM3.1 T47 runs 2 and 3 and HadCM3 (Table III). This bias is subsequently reflected in the multi-model 1900–1999 means for all emission scenarios (Table II). The GCMs split between those showing a shift, often significant, towards more negative PDO-like conditions for all three scenarios (i.e. MIROC (medres), MRI and HadCM3) and those showing a contrary shift, also often significant, towards more positive PDO-like conditions for all runs and all three scenarios (i.e. CGCM3.1 (T47), CGCM3.1 (T63), GDFL2.1, MIROC (hires) and PCM) (Table III). The ECHAM5 runs slightly favoured negative PDO-like conditions and CCSM3 splits according to emissions scenario. The tendencies of the individual GCMs for one PDO phase or the other largely continued unchanged if extended to 2051–2099. Inspection

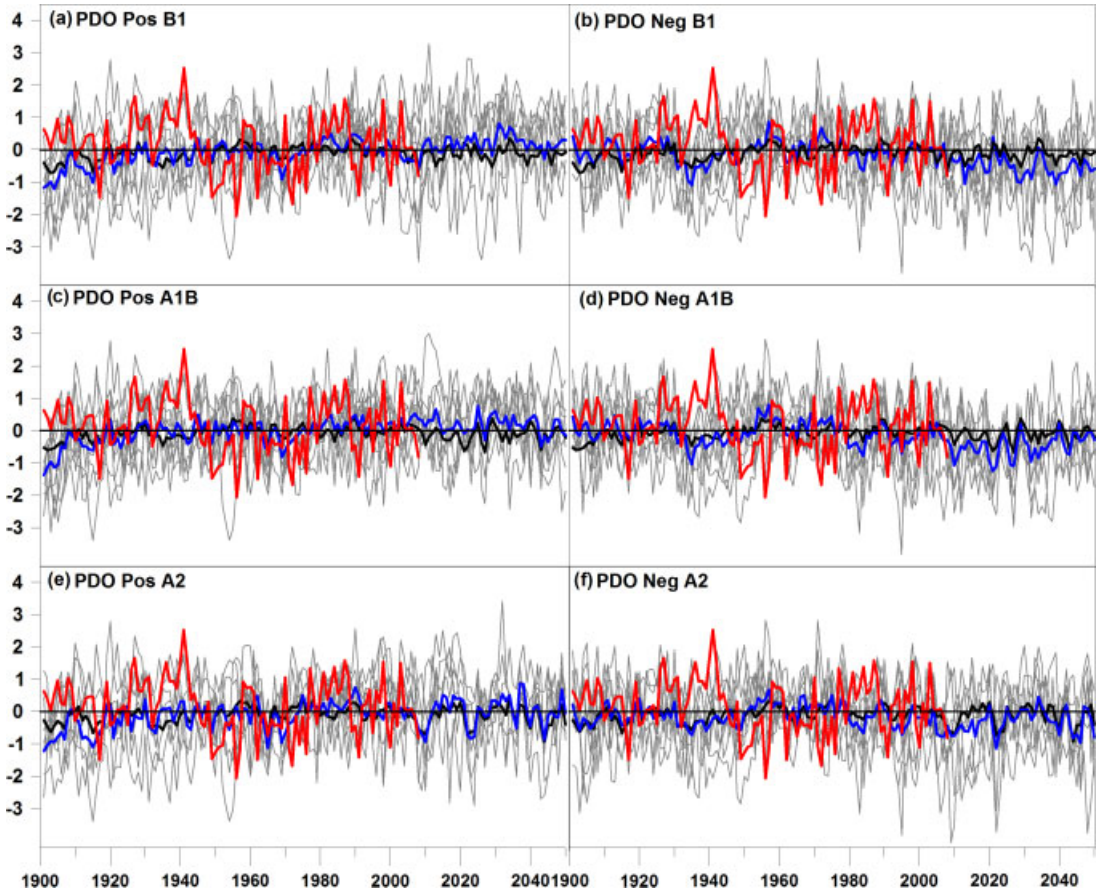

Figure 4. Winter averaged (November to March) PDO indices 1900–1999 calculated from 20th-century simulations, together with projections for 2000–2050 for the B1, A1B and A2 emission scenarios. Panels (a), (c), and (e) show the GCM runs that showed a positive shift in the 2000–2050 mean relative to the corresponding 1900–1999 mean (Table III). Panels (b), (d), and (f) show the GCM runs that showed a negative shift in the 2000–2050 mean relative to the corresponding 1900–1999 mean (III). The grey lines are the individual model runs, the heavy blue lines are multi-model means of the individual GCM runs shown in that panel and the heavy black lines are the multi-model means of all the GCMs. Also shown in red is the observed PDO based upon HadSST2 data. This figure is available in colour online at wileyonlinelibrary.com/journal/joc

Table II. Twentieth-century observed mean climate indices and multi-model mean climate indices for the 20th-century simulations and for the 21st-century projections under the B1, A1B and A2 SRES emission scenarios.

	Winter PDO			June to November SOI			Winter NAO		
SRES emission scenario	B1	A1B	A2	B1	A1B	A2	B1	A1B	A2
Observed mean 1900–1999	0.168	0.168	0.168	−0.098	−0.098	−0.098	0.485	0.485	0.485
All-model 1900–1999 simulation mean[b]	−0.109	−0.075	−0.101	0.061	0.066	0.063	−0.059	−0.050	−0.060
All-model 2000–2050 mean	**−0.130**	**−0.095**	**−0.129**	*−0.022*	*0.006*	*0.009*	**−0.019**	**0.115**	**0.101**
All-model 2000–2099 mean	**−0.161**[a]	**−0.162**	**−0.321**	*−0.017*	*0.052*	**0.089**	**−0.040**	**0.177**	**0.161**

Italic values identify a future shift to a positive PDO or negative SOI (El Niño-like) or negative NAO mean state; and bold to the opposite conditions (*i.e.*, negative PDO or positive SOI (La Niña-like) or positive NAO), relative to the 20th-century simulation mean. Underscore denotes a significant change in a multi-model mean index at the $p \leq 0.05$ level, relative to the 20th-century simulation mean, as assessed by a Monte Carlo t-test.

[a] denotes significant change at the $0.05 < p \leq 0.10$ level.

[b] Not all GCMs had 21st-century projected data for all three emission scenarios, therefore their simulation runs were dropped from the multi-model simulation mean where applicable.

of the plots of the projected PDO for individual runs suggests that the mean shifts were due to the projections drifting to one phase or the other and not to variance changes, particularly not to changes in the number of low extreme values relative to the number of high extremes.

Early 21st century (2000–2050) June to November SOI projections showed a shift towards a climate with more El Niño-like conditions (negative SOI) and decreases in La Niña-like conditions (positive SOI) for all three emissions scenarios (Tables II and III). Under the B1 and A1B scenarios, the shift towards more El

Table III. The average winter PDO, June to November SOI and winter NAO indices for the simulated 20th-century runs 1900–1999 (20c3m) and for the projected runs for 2000–2050 for each climate model and emissions scenario.

GCM No.	GCM Run	PDO				SOI				NAO			
		20c3m	B1	A1B	A2	20c3m	B1	A1B	A2	20c3m	B1	A1B	A2
1	**CGCM3.1 T47_1**	−0.22	*−0.05*	*−0.11*	*−0.11*	0.01	*−0.10*	*−0.03*	*−0.11*	−0.11	**0.21**[a]	**0.33**	**0.25**[a]
1	**CGCM3.1 T47_2**	0.29	*0.69*	*0.75*	*0.51*	0.09	*0.01*	*−0.13*[a]	*0.05*	−0.01	**0.27**	**0.30**[a]	**0.45**
1	**CGCM3.1 T47_3**	0.28	*0.99*	*0.66*	*0.67*	−0.04	**0.06**	**0.01**	*−0.04*	−0.02	*−0.10*	−0.19	−0.02
2	**CGCM3.1 T63**	−0.11	*0.36*	*0.08*	na	0.12	**0.46**	**0.22**	na	−0.06	**0.20**	*−0.19*	na
3	**ECHAM5_1**	−0.42	*−0.36*	*−0.13*	**−0.52**	0.10	**0.18**	**0.13**	*−0.03*	0.08	**0.27**	**0.35**	**0.60**
3	**ECHAM5_2**	0.04	na	**−0.17**	na	0.01	na	*−0.05*	na	−0.19	na	**0.14**	na
3	**ECHAM5_3**	−0.21	**−0.25**	na	na	0.04	*−0.07*	na	na	−0.09	*−0.11*	na	na
4	**GDFL2.1**	−0.36	*−0.18*	*−0.01*	*−0.22*	0.05	**0.19**	**0.21**	**0.12**	−0.21	**−0.16**	**0.19**	**0.04**
5	**MIROC(hires)**	−0.13	*0.58*	*0.50*	na	−0.01	*−0.82*	*−0.66*	na	−0.01	*−0.05*	**0.00**	na
6	**MIROC(medres)**	−0.18	**−0.23**	**−0.53**	**−0.45**[a]	0.29	*0.07*[a]	*0.18*	*0.11*	0.03	**0.08**	*−0.06*	*0.02*
7	**MRI-2.3.2_1**	−0.15	**−0.91**	**−0.40**	**−0.19**	−0.09	*−0.19*	*−0.16*	*−0.27*	0.00	**0.30**	**0.03**	*−0.41*[a]
7	**MRI-2.3.2_2**	0.03	**−0.05**	**−0.07**	**−0.03**	0.00	*−0.12*	*−0.01*	**0.01**	0.04	*−0.14*	**0.12**	**0.07**
7	**MRI-2.3.2_3**	0.02	**−0.40**	**−0.49**	**−0.48**	0.18	*−0.11*[a]	*0.05*	*0.00*	−0.05	*−0.19*	**-0.02**	**0.06**
7	**MRI-2.3.2_4**	0.06	**−0.29**	**−0.48**	**−0.13**	0.14	*−0.14*	*0.01*	*−0.16*	−0.24	**0.51**	**−0.07**	**−0.02**
7	**MRI-2.3.2_5**	−0.45	**−1.02**	**−0.61**	**−0.45**	0.04	*−0.18*	*−0.03*	*−0.02*	−0.10	*−0.31*	**−0.04**	**0.06**
8	**NCAR-CCSM3**	0.15	**−0.41**	na	*0.20*	−0.09	**−0.05**	na	**−0.03**	−0.25	**0.07**[a]	na	**0.03**[a]
9	**NCAR-PCM_1**	−0.67	*−0.54*	na	*−0.30*	0.06	**0.13**	na	*−0.08*	0.16	*0.06*	na	**0.29**
9	**NCAR-PCM_3**	−0.07	na	*0.11*	na	0.03	na	*−0.02*	na	0.22	na	**0.50**[a]	na
9	**NCAR-PCM_4**	−0.16	*0.13*	*−0.11*	*−0.02*	−0.02	*−0.07*	*−0.13*	**0.16**[a]	−0.21	*−1.09*	**0.15**	**0.30**
10	**HadCM3**	0.25	**−.40**	**−0.60**	**−0.42**	0.20	**0.37**	**0.50**[a]	**0.41**	0.00	*−0.16*	**0.15**	*−0.21*

Italic values identify future simulations that shift to a positive PDO or negative SOI (El Niño-like) or negative NAO mean state; and bold to the opposite conditions (*i.e.*, negative PDO or positive SOI (La Niña-like) or positive NAO), relative to the 20th-century simulation mean. GCMs ordered as in Table I. Underscore denotes a significant change in the 2000–2050 mean index at the $p \leq 0.05$ level, relative to the 20th-century simulation mean, as assessed by a Monte Carlo t-test.

[a] denotes significant change at the $0.05 < p \leq 0.10$ level.

"na" means no run was archived for that emissions scenario.

Niño-like conditions was significant at the $p \leq 0.05$ level and under the A2 scenario the shift was non-significant ($p > 0.1$). Comparison of the 20th-century simulation means to the actual observed mean SOI index showed that all GCMs had a slight bias towards simulating more La Niña conditions than actually happened. The MIROC3.2 (hires and medres) models showed a shift towards more El Niño-like conditions for all emissions scenarios, whereas the MRI and CGCM3.1 (T47) models showed a similar shift towards more El Niño-like conditions in most runs and scenarios (Table III). The CGCM3.1 (T63), GFDL 2.1, CCSM3 and HadCM3 models showed a shift towards more La Niña-like conditions for all scenarios. The NCAR-PCM and ECHAM5 runs split between El Niño- and La Niña-like conditions, depending on the scenario. Using the annual SOI gave similar results in all analyses and is therefore not discussed further.

The early 21st century (2000–2050) NAO projections for all three scenarios showed a shift towards a climate with more occurrences of the positive NAO phase (positive AO) relative to the negative NAO (negative AO), significant at the $p \leq 0.05$ level for the A1B and A2 scenarios and not significant for the B1 scenario (Tables II and III). Comparison of the 20th-century simulation means to the actual observed mean NAO index showed that the GCMs had a problem reproducing the NAO accurately, having a marked bias towards simulating more negative NAO events than actually happened for all emissions scenarios. The CGCM3.1 (T63), GDFL2.1 and NCAR-CCSM3 means showed a shift towards more positive NAO conditions for all three emissions scenarios, whereas the CGCM3.1 (T47), ECHAM5, MRI and NCAR-PCM run means favoured a shift towards more positive NAO conditions, particularly for the A1B and A2 scenarios, and towards more negative NAO conditions for the B1 scenario (Table III). Negative NAO-like conditions were favoured more by MIROC (hires), MIROC (medres) and HadCM3.

The observed PDO pattern is still present in the same form in the projected 2000–2050 North Pacific. This is shown by comparing EOF 1 of a PCA of the 2000–2050 residual SST anomalies to the observed 1900–1993 PDO pattern (Figures 5–7 and Table VI). For all three emission scenarios, almost all runs of the models produced a recognizable PDO spatial pattern as their EOF 1, which had a spatial correlation of at least 0.70 with the observed PDO pattern. The two exceptions, CGCM3.1 (T47) run 2 and MIROC (medres), had EOFs with a spatial correlation of 0.69, which does not seem markedly inferior (Table VI) (for brevity, if multiple runs were available for a model, ensemble means are presented

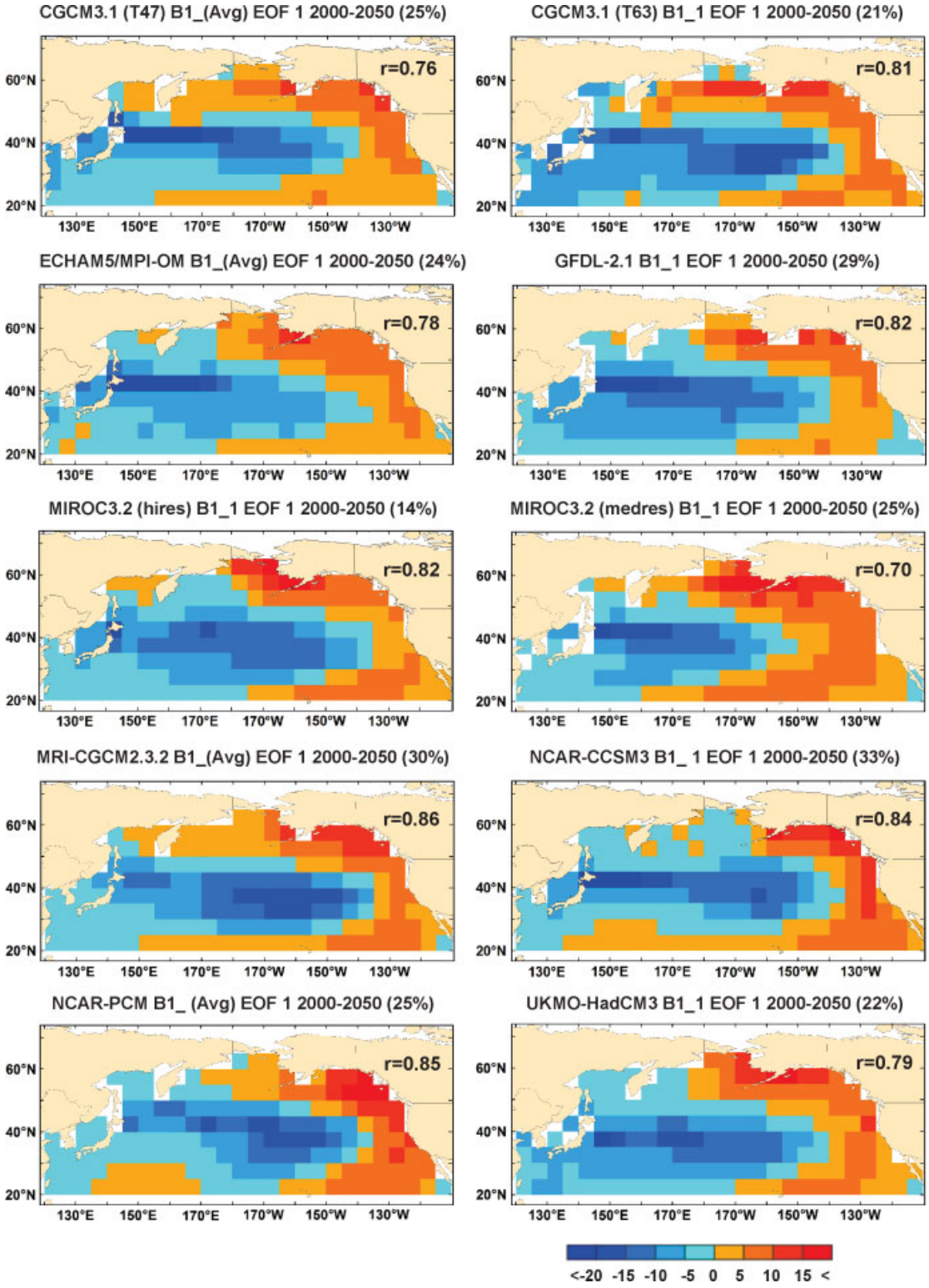

Figure 5. The spatial patterns of EOF 1 of the 2000–2050 North Pacific projected SST residuals from the ten models with available runs, under the 21st-century B1 emissions scenario. If multiple runs were available for a model, ensemble means are presented. The percent variance explained is given after the model name; spatial correlation coefficients from comparison to the 1900–1993 observed PDO pattern indicated in the upper right hand corner. Color scale shows PCA loadings (×100). This figure is available in colour online at wileyonlinelibrary.com/journal/joc

in the figures, but the individual runs were checked). Similar to the simulated 20th-century PDO patterns, the early 21st-century PDOs also typically explained more North Pacific residual variance, the exception again being MIROC (hires) (Figures 1 and 5–7).

All the GCMs had some capacity to produce the characteristic spectrum of the PDO: the lowest frequency pentadecadal (50–70 years) periodicity and the low-frequency bidecadal (15–20 years) periodicity, and higher frequency variability in the ENSO band of

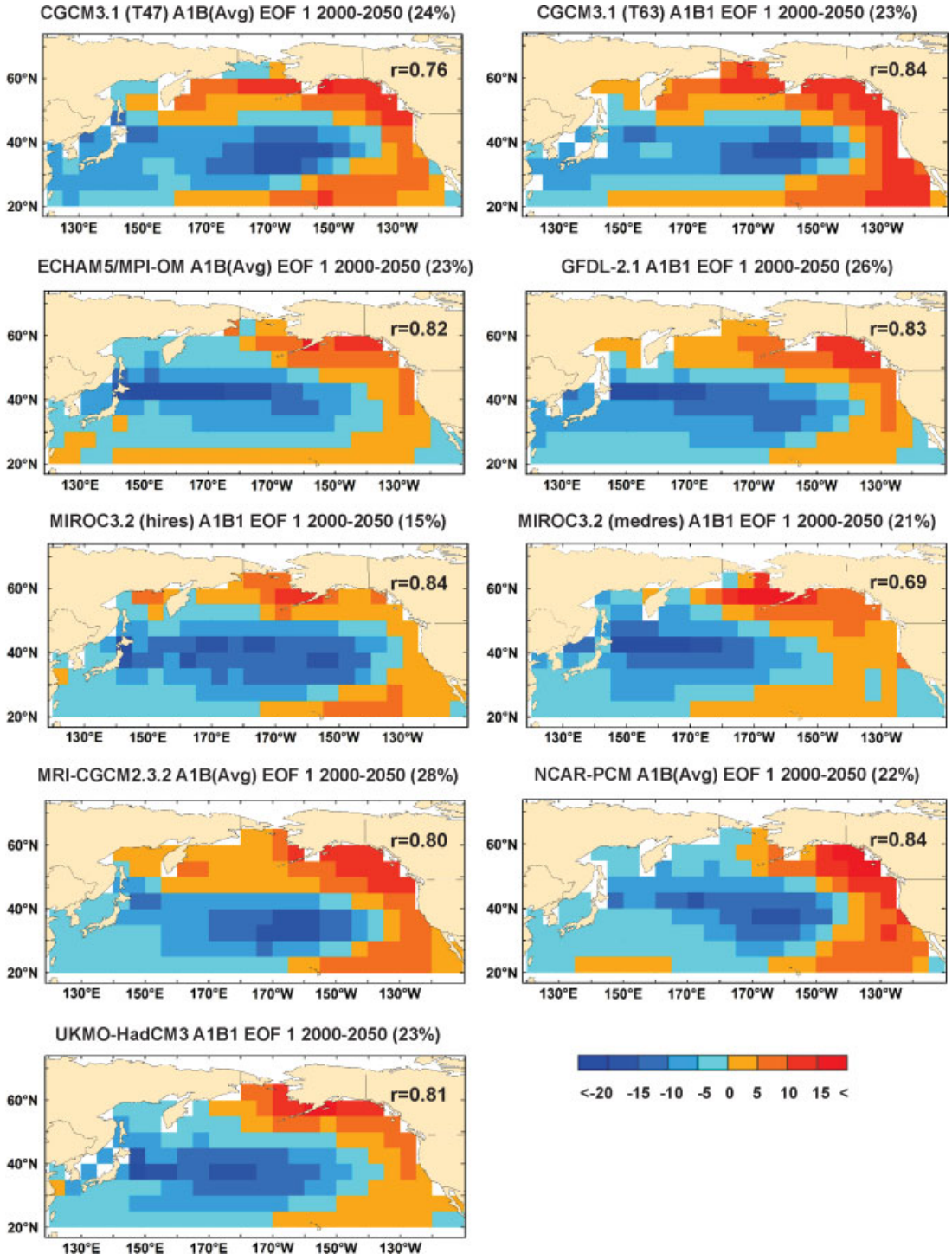

Figure 6. The spatial patterns of EOF 1 of the 2000–2050 North Pacific projected SST residuals from the nine available models, under the 21st-century A1B emissions scenario. If multiple runs were available for a model, ensemble means are presented. The percent variance explained is given after the model name; spatial correlation coefficients from comparison to the 1900–1993 observed PDO pattern indicated in the upper right hand corner. Color scale shows PCA loadings (×100). This figure is available in colour online at wileyonlinelibrary.com/journal/joc

2–7 years (Minobe, 1999) (Table IV and VI). However, typically the pentadecadal and bidecadal peaks were shifted towards higher frequencies, as were the ENSO bands. All the available pre-industrial control runs showed power in two low-frequency bands that appeared analogous to the pentadecadal and bidecadal peaks, except for MIROC (hires) which showed only the lowest frequency peak. Typically, the 20th-century simulation runs had no significant variability that corresponded to the pentadecadal peak; their length was too short to reasonably detect it. Almost all 20th-century simulation runs had significant variability that corresponded to the bidecadal peak and all had the ENSO band, almost invariably shifted to higher frequencies. We considered a GCM to have reasonably PDO-like spectral properties if at least one of its pre-industrial control or 20th-century

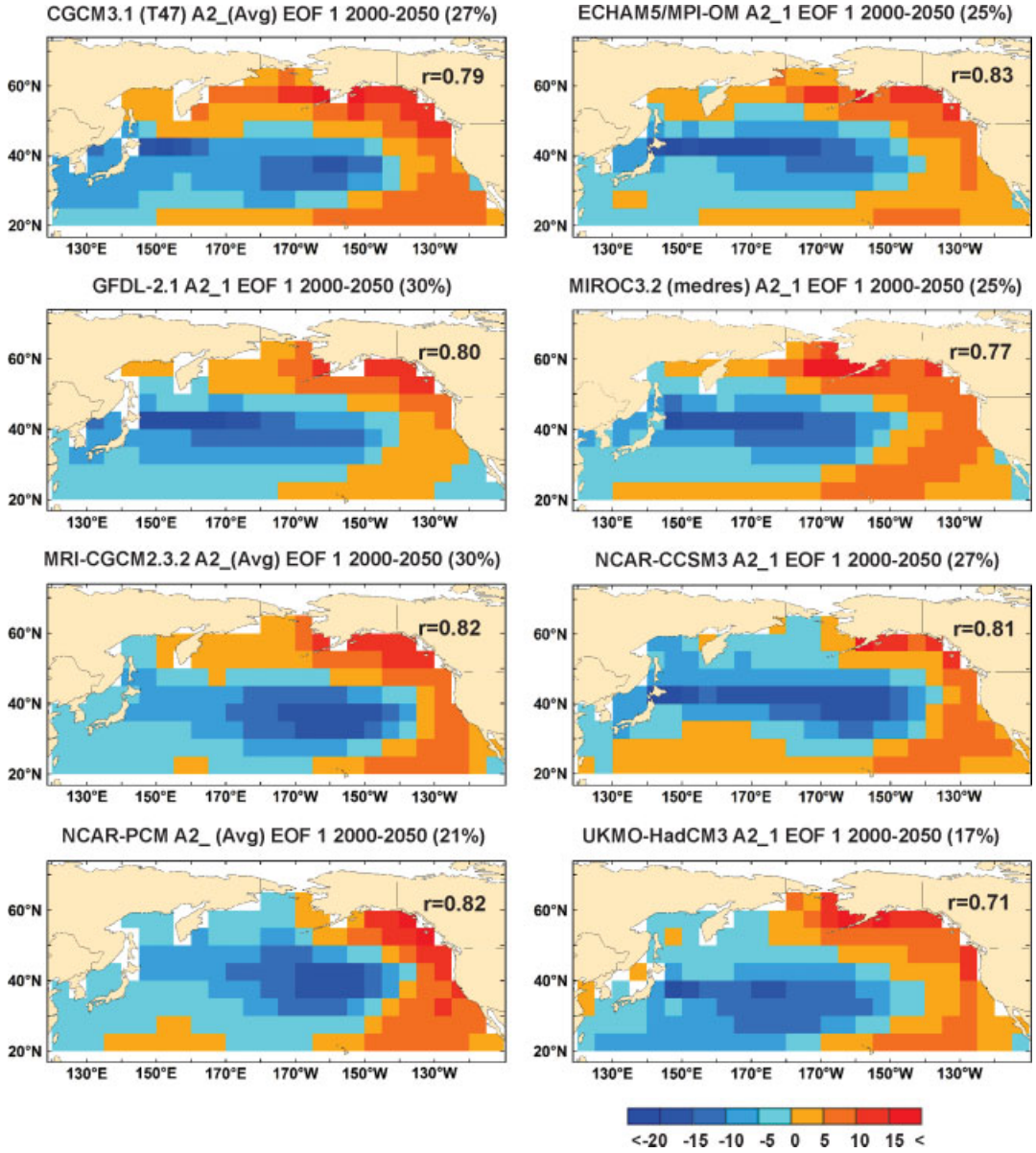

Figure 7. The spatial patterns of EOF 1 of the 2000–2050 North Pacific projected SST residuals from the eight models with available runs, under the 21th-century A2 emissions scenario. If multiple runs were available for a model, ensemble means are presented. The percent variance explained is given after the model name; spatial correlation coefficients from comparison to the 1900–1993 observed PDO pattern indicated in the upper right hand corner. Color scale shows PCA loadings (×100). This figure is available in colour online at wileyonlinelibrary.com/journal/joc

simulation runs had pentadecadal, bidecadal and ENSO band analogues. By this criterion, nine of the ten remaining GCMs demonstrated ability to produce a PDO-like spectrum (Table VI). The exception was ECHAM5, which did not show pentadecadal variability in its 20th-century runs and had no pre-industrial runs. Since the 20th-century runs are potentially too short to detect the lowest frequencies, the ECHAM5 model was kept.

Comparison of the frequencies of the in-phase PDO/ENSO occurrences and the out-of-phase PDO/ENSO occurrences in the observed data to those in the 20th-century simulated runs demonstrated that all GCMs replicated the temporal coherence between the PDO and ENSO well. The exceptions were CGCM3.1 (T47) runs 1 and 2 which did not and CGCM3.1 (T63) and MRI run 3 which were borderline (Tables V and VI). Comparison of the frequencies of the in-phase PDO/ENSO occurrences and the out-of-phase PDO/ENSO occurrences in the projected data for 2000–2050 for each emissions scenario to those in the corresponding 20th-century simulation runs demonstrated that 32% of the GCM runs changed the temporal coherence between the PDO and ENSO in 2000–2050 relative to 1900–1999 (Table V).

4. Discussion

The status of the PDO in a warmer world under anthropogenic climate change is of serious concern because it reflects an integrated metric of the North Pacific atmosphere-ocean system given its influence on North

Table IV. Summary of GCM performance in producing the characteristic spectra of the winter PDO, using the pre-industrial control runs and the 20th-century simulation runs.

GCM No.	GCM Run	Pre-industrial spectra			20th-century spectra		
		Lowest frequency PDO band (50–70 yr)	Low- frequency PDO band (15–20 yr)	ENSO band (2-7yr)	Lowest frequency PDO band (50–70 yr)	Low-frequency PDO band (15–20 yr)	ENSO band (2–7 yr)
1	**CGCM3.1 T47_1**	21.3	12.5	2.4–7.3	31.7[a]	11.1, 16.4	2.9–3.7
1	**CGCM3.1 T47_2**	21.3	12.5	2.4–7.3	none	8.7	2.1–3.7
1	**CGCM3.1 T47_3**	21.3	12.5	2.4–7.3	none	8.8, 16.8	2.3–4.0
2	**CGCM3.1 T63**	36.6	13.0	2.1–7.4	none	8.3, 17.3	2.1–4.4
3	**ECHAM5_1**	na	na	na	none	9.7–11.9	4.0–5.0
3	**ECHAM5_2**	na	na	na	none	none	2.9–3.7
3	**ECHAM5_3**	na	na	na	none	11.8[a]	3.2[a]–7.9
4	**GDFL2.1**	52.5[a]	11.5[a], 19.6	2.3–5.3	49.5	14.1[a]	2.7–4.9[a]
5	**MIROC(hires)**	33.7	none	2.5	49.5	16.8	2.0–5.3
6	**MIROC(medres)**	35.3	11.9[a]	2.4–7.4	28.2[a]	7.4[a], 9.0[a]	2.5–5.3
7	**MRI-2.3.2_1**	29.3	10.9	2.1–5.5	none	20.1–28.2	2.0–6.9
7	**MRI-2.3.2_2**	29.3	10.9	2.1–5.5	28.2	16.1	2.3–5.5
7	**MRI-2.3.2_3**	29.3	10.9	2.1–5.5	none	none	2.3–5.6
7	**MRI-2.3.2_4**	29.3	10.9	2.1–5.5	none	10.3	2.6–4.1
7	**MRI-2.3.2_5**	29.3	10.9	2.1–5.5	none	18.3	2.3–3.7
8	**NCAR-CCSM3**	25.0	8.5, 12.5	2.0–6.9	none	11.3–16.5	2.1–2.9
9	**NCAR-PCM_1**	na	na	na	49.5	17.9–21.5	2.0–5.1
9	**NCAR-PCM_3**	na	na	na	none	none	2.5–5.6
9	**NCAR-PCM_4**	na	na	na	none	8.8–11.8	2.3–3.7
10	**HadCM3**	31.7[a]	13.5	2.4–5.7	none	12.2–20.5	3.3–3.5

Multi-taper spectral analysis was used (five tapers for the long pre-industrial runs and three tapers for the shorter 20th-century simulation runs). Shown are the periodicities (in years) of significant peaks at the 0.10 significance level using adaptively weighted spectra with a red noise background (Mann and Lees, 1996). "na" means no run was archived.
[a] denotes a peak that is barely insignificant.

Pacific Ocean physical forcing and marine ecology and strong correlations with present day North Pacific climatology and hydrology. The capacities of the current highest resolution GCMs to project the future status of the PDO are just beginning to be examined. As far as we know, our present study is the first to explicitly project the PDO, as calculated by EOF analysis of North Pacific SST residuals. This analysis of PDO projections for 2000–2050 shows a multi-model mean shift towards more occurrences of the negative phase PDO. Some form of the correlates or effects of a multi-model mean result of more negative phase PDO-like conditions for the early 21st century may be apparent throughout the North Pacific Basin, as long as the PDO's regional teleconnections maintain stationarity (Mantua and Hare, 2002; Deser *et al*., 2004; Pavia *et al*., 2006). In general, this shift towards more negative PDO-like conditions in the North Pacific Basin will be superimposed upon the general global warming trend and its meridional pattern of differing effects from hydrological cycle intensification, i.e. drying in mid-latitude and sub-tropical regions and increasing moisture in northern regions.

However, this multi-model mean result of more negative phase PDO-like conditions for the early 21st century is relatively weak; it is non-significant, although it becomes significant if the entire 21st century is examined (Table II). The GCMs separate between those showing a shift, often significant, towards more negative PDO-like conditions for all three scenarios [i.e. MIROC (medres), MRI and HadCM3] and those showing a contrary shift, also often significant, towards more positive PDO-like conditions for all runs and all three scenarios [i.e. CGCM3.1 (T47), CGCM3.1 (T63), GDFL2.1, MIROC (hires) and NCAR-PCM] (Table III). Confidence in a projected negative PDO shift would be higher if the GCMs showed more consistency, and also if the physical basis for the PDO was better understood, and a projected negative PDO shift made sense in this mechanistic context. Except for CGCM3.1 T47 runs 1 and 2, the ten GCMs showed the observed 20th-century coherence between the PDO and ENSO (Table VI) and did a reasonable job at producing a PDO-like spectrum. Removal of these two positive-trending runs which did not show the required observed 20th-century coherence between the PDO and ENSO from the multi-model mean does strengthen the result of the negative PDO shift for the 21st century. As well, multi-model averaging serves to filter out biases of the individual models and its results are often in better agreement with observations than simulations from individual models (IPCC4, 2007); hence,

Table V. Comparison of the frequencies of the in-phase positive PDO/El Niño and negative PDO/La Niña occurrences and the out-of-phase positive PDO/La Niña and negative PDO/El Niño occurrences in the 20th-century simulation (20c3m) runs for each chosen GCM versus these same frequencies in the observed data for 1900–1999. Also shown are comparisons of the frequencies of the in-phase PDO/ENSO occurrences and the out-of-phase PDO/ENSO occurrences in the 20th-century simulated runs versus those in the corresponding projected data for 2000–2050 for each emissions scenario.

GCM No.	GCM Run	20c3m	B1	A1B	A2
1	**CGCM3.1 T47_1**	$p \leq 0.05$	no change	no change	$p \leq 0.05$
1	**CGCM3.1 T47_2**	$p \leq 0.05$	$p \leq 0.05$	$p \leq 0.05$	no change
1	**CGCM3.1 T47_3**	no change	$p \leq 0.05$	no change	$p \leq 0.05$
2	**CGCM3.1 T63**	$0.05 < p \leq 0.1$	$p \leq 0.05$	no change	na
3	**ECHAM5_1**	no change	no change	no change	no change
3	**ECHAM5_2**	no change	na	no change	na
3	**ECHAM5_3**	no change	no change	na	na
4	**GDFL2.1**	no change	$p \leq 0.05$	no change	no change
5	**MIROC(hires)**	no change	$p \leq 0.05$	$p \leq 0.05$	na
6	**MIROC(medres)**	no change	no change	$0.05 < p \leq 0.1$	no change
7	**MRI-2.3.2_1**	no change	no change	no change	no change
7	**MRI-2.3.2_2**	no change	no change	no change	no change
7	**MRI-2.3.2_3**	$0.05 < p \leq 0.1$	no change	$0.05 < p \leq 0.1$	$p \leq 0.05$
7	**MRI-2.3.2_4**	no change	no change	no change	no change
7	**MRI-2.3.2_5**	no change	$p \leq 0.05$	no change	no change
8	**NCAR-CCSM3**	no change	no change	na	no change
9	**NCAR-PCM_1**	no change	$p \leq 0.05$	na	no change
9	**NCAR-PCM_3**	no change	na	no change	na
9	**NCAR-PCM_4**	no change	$p \leq 0.05$	no change	no change
10	**HadCM3**	no change	no change	$p \leq 0.05$	$p \leq 0.05$

Chi-square tests were used to assess significance of frequency changes. A strong PDO occurrence was defined as |winter PDO| > 0.7 standard deviations, and a strong to moderate ENSO event was defined as |June to November SOI| > 0.5. "na" means no run was archived for that emissions scenario. GCMs ordered as in Table I.

the multi-model mean shift towards negative PDO-like conditions should be seriously considered.

Research on the future state of the PDO is preliminary. Oshima and Tanimoto (2009) examined the spatial and temporal patterns of the PDO in the 20th-century GCM simulations and 21st-century projections; however, they defined the PDO index by an area weighted average of the SST anomalies over a single, homogeneous centre of action in the central North Pacific region, i.e. without using residual EOF analysis. Their method cannot differentiate between the general anthropogenic global temperature increase and a multi-model mean shift towards more negative PDO-like conditions in the North Pacific. Overland and Wang (2007) and Wang *et al.* (2010) found that the global warming trend will surpass the natural variability circa 2040–2050 under the A1B emissions scenario, leading to a weaker meridional temperature gradient in the North Pacific region. Because of their result, we do not emphasize PDO projections past 2050. Their EOF analysis used direct North Pacific SST anomalies, rather than the residuals after the global ocean warming trend had been removed, as did our analysis, which followed that of Mantua *et al.* (1997) and Zhang *et al.* (1997). We note that the leading mode in the 21st century from Overland and Wang (2007) was a more homogeneous pattern than ours, due to their different method based on SST anomalies, rather than SST residuals, and PC analysis for the entire 21st century. Because of space limitations, the projection of EOF 2 of the observed North Pacific residual SSTs (the Victoria pattern) and the related North Pacific Gyre Oscillation is outside the scope of this paper (Bond *et al.*, 2003; Di Lorenzo *et al.*, 2008; Overland *et al.*, 2008; Whitfield *et al.*, 2010).

It is important to verify that these negative PDO shifts of the individual GCM runs are not an artefact of the projection method. Even after the global mean ocean SST anomaly time series has been subtracted off the North Pacific SST anomalies, it is conceivable that a large amount of global warming could remain in the North Pacific residuals. This is because the global mean ocean SST anomaly time series is weighted towards the tropics, where warming will not be as great as in the higher latitudes (IPCC 4, 2007; their Figure 10.8). If a more or less spatially homogeneous warming pattern still exists in the North Pacific residuals, it could potentially induce a shift towards negative PDO-like conditions as an artefact, because of the method used to project the PDO into the 21st century (matrix multiplication of the 20th century EOF 1) since the western pole of the PDO loading pattern extends over a large area.

In order to rule out this potential problem, we examined plots of the differences between North Pacific SST anomalies and residuals for 1950–1959 *versus* 2040–2049 for all three emissions scenarios. Global

Table VI. Summary of GCM performance in producing the PDO.

GCM No.	GCM Run	2000–2050 EOF 1 = PDO pattern?			Pre-industrial spectra	20th-century spectra	20th-century coherence with ENSO
		B1	A1B	A2			
1	**CGCM3.1 T47_1**	yes	yes	yes	fine	fine	no
1	**CGCM3.1 T47_2**	yes	yes	no[a]	fine	no pentadecadal	no
1	**CGCM3.1 T47_3**	yes	yes	yes	fine	no pentadecadal	yes
2	**CGCM3.1 T63**	yes	yes	na	fine	no pentadecadal	yes
3	**ECHAM5_1**	yes	yes	yes	na	no pentadecadal	yes
3	**ECHAM5_2**	na	yes	na	na	no bidecadal, no pentadecadal	yes
3	**ECHAM5_3**	yes	na	na	na	no pentadecadal	yes
4	**GDFL2.1**	yes	yes	yes	fine	fine	yes
5	**MIROC(hires)**	yes	yes	na	no bidecadal	fine	yes
6	**MIROC(medres)**	yes	no[a]	yes	fine	fine	yes
7	**MRI-2.3.2_1**	yes	yes	yes	fine	no pentadecadal	yes
7	**MRI-2.3.2_2**	yes	yes	yes	fine	fine	yes
7	MRI-2.3.2_3	yes	yes	yes	fine	no bidecadal, no pentadecadal	yes
7	**MRI-2.3.2_4**	yes	yes	yes	fine	no pentadecadal	yes
7	**MRI-2.3.2_5**	yes	yes	yes	fine	no pentadecadal	yes
8	**NCAR-CCSM3**	yes	na	yes	fine	no pentadecadal	yes
9	**NCAR-PCM_1**	yes	na	yes	na	fine	yes
9	**NCAR-PCM_3**	na	yes	na	na	no bidecadal, no pentadecadal	yes
9	**NCAR-PCM_4**	yes	yes	yes	na	no pentadecadal	yes
10	**HadCM3**	yes	yes	yes	fine	no pentadecadal	yes

The 2000–2050 EOF 1 = PDO pattern as assessed in Figures 5–7, *i.e.*, that the spatial correlation (r) between EOF 1 of the 2000–2050 residual projected SST anomalies and the PDO loading pattern (EOF 1) from the 1900–1993 observed data was ≥ 0.70; spectra are listed as "fine" if pentadecadal, bidecadal and ENSO band variability analogs are found (Table IV), 20th-century coherence with ENSO as assessed in Table V, *i.e.*, do the 20th-century simulation runs contain frequencies of in-phase and out-of-phase PDO/ENSO events comparable to those of the observed 20th-century record? "na" means no run was archived for that emissions scenario. GCMs ordered as in Table I.

[a] $r = 0.69$.

warming of 1–3 °C, often in a more or less spatially homogeneous warming pattern, as in CGCM3.1 T47 (all scenarios), CGCM3.1 T63 (B1 and A1B), MIROC3.2 (hires) (B1) and MIROC3.2 (medres) (A1B and A2), is clearly present in the plots of the differences between the average SSTs in the 1950s from that in the 2040s (Figure 8 shows the anomaly difference plot for the A1B scenario, the other scenarios are similar). However, examination of the plots of the differences between North Pacific SST residuals for 1950–1959 *versus* 2040–2049 (Figure 9 shows the residual difference plot for the A1B scenario, the other scenarios are similar) shows that the unsophisticated method of removing global warming by subtracting the global mean ocean SST anomaly time series works quite well, removing any obvious global warming pattern. In particular, the spatially homogeneous warming pattern in CGCM3.1 T47 (A1B, A2), CGCM3.1 T63 (B1 and A1B), MIROC3.2 (hires) (B1) and MIROC3.2 (medres) (A1B and A2) is removed. The spatially homogeneous warming pattern in CGCM3.1 T47 (B1) does remain, but this model actually shows a positive shift in the PDO index for this scenario. Hence, this issue of the negative PDO shift as an artefact of the projection method does not appear to be a problem.

The exact nature of the couplings among the extratropical North Pacific Ocean, its overlying atmosphere, and their mutual downstream atmospheric teleconnections is an active research area. Some hypothesize that North Pacific Ocean SST variability significantly affects the overlying atmospheric circulation given the ocean's greater thermal inertia (Bond and Harrison, 2000; Rodionov *et al.*, 2007). Others hypothesize that the North Pacific atmospheric circulation drives the underlying mixed-layer oceanic variability, noting, for instance, that the correlations between North Pacific SST and SLP are strongest when the atmosphere leads the ocean by several months (Davis, 1976; Trenberth and Hurrell, 1994; Lau, 1997; Kushnir *et al.*, 2002). The crux of the matter is the sensitivity of the non-boundary layer middle latitude atmosphere to slower SST variability (Overland *et al.*, 2010). Much evidence, often GCM-based, suggests that the SST feedback on the mid-latitude atmosphere is small compared to internal atmospheric variability (Trenberth and Hurrell, 1994; Lau, 1997; Kushnir *et al.*, 2002), except potentially in the region of the western boundary currents (Minobe *et al.*, 2008). As a possible mechanism to explain the North Pacific atmospheric low-frequency variability, Dima and Lohmann (2007) suggest that variations in the thermohaline circulation produce low-frequency uniform anomalies in North Atlantic SSTs (the Atlantic Multidecadal Oscillation) that

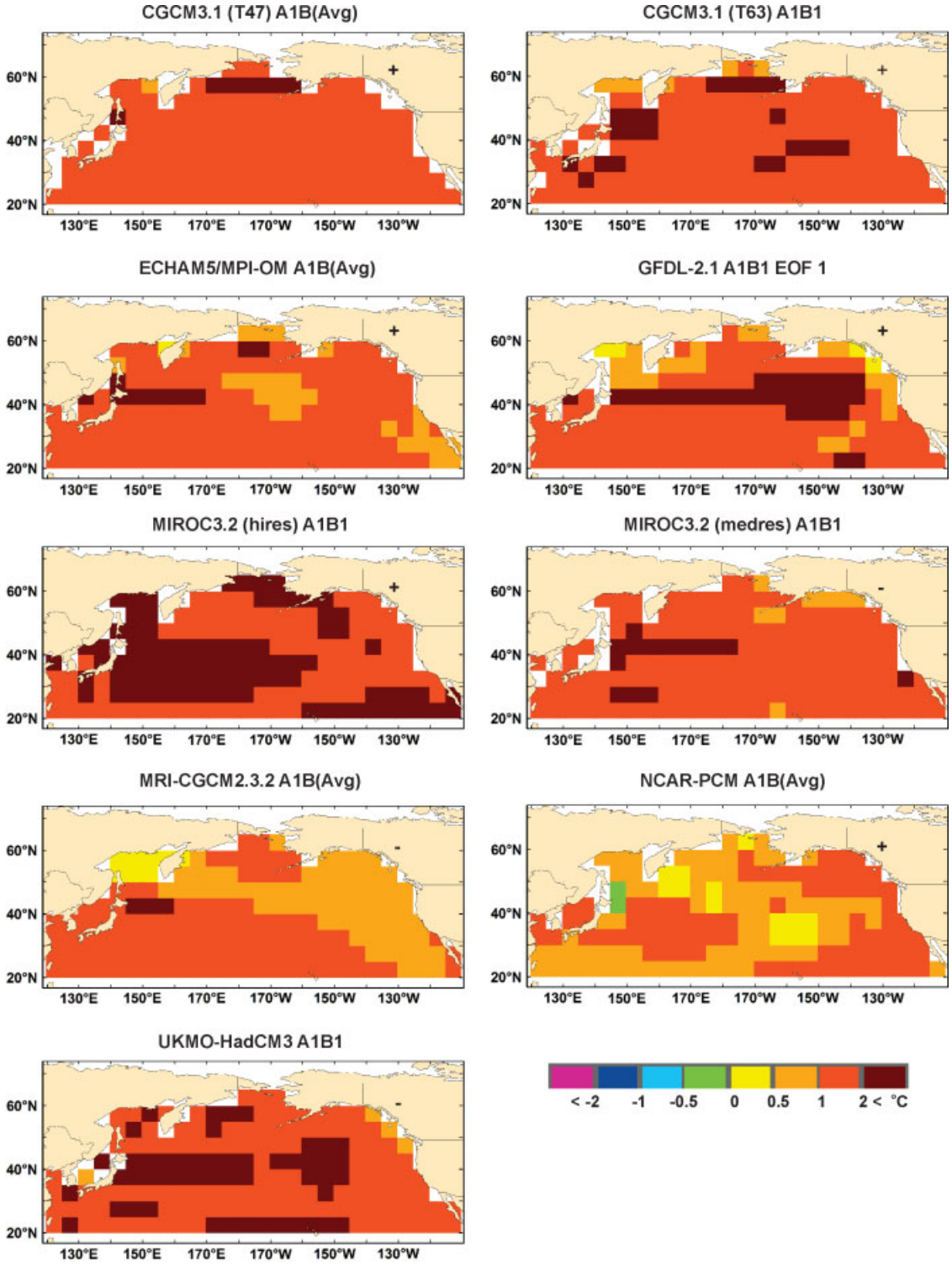

Figure 8. Plots of the differences between North Pacific SST anomalies (°C) for 1950–1959 *versus* 2040–2049 for the A1B emissions scenario for each GCM. As a look-up aid, the plus or minus sign over the Yukon Territory, Canada, denotes whether a particular GCM run or average run showed a positive PDO shift (+) or negative PDO shift (−) in the 21st century as in Table III. This figure is available in colour online at wileyonlinelibrary.com/journal/joc

are associated with a hemispheric SLP pattern that shows opposite atmospheric pressure anomalies over the North Pacific and North Atlantic Oceans (see review in McCabe *et al*., 2008). This North Pacific SLP pattern is amplified through atmosphere-ocean interactions and the SST pattern appears to be the PDO.

The mechanism by which the PDO, or the zonal dipole in North Pacific SSTs, affects the hydroclimatology of the downstream western North America is through a shift in the position of the sub-polar jet, which brings winter storms and precipitation as it crosses over the edge of the continent (Gershunov and Barnett, 1998; Bonsal

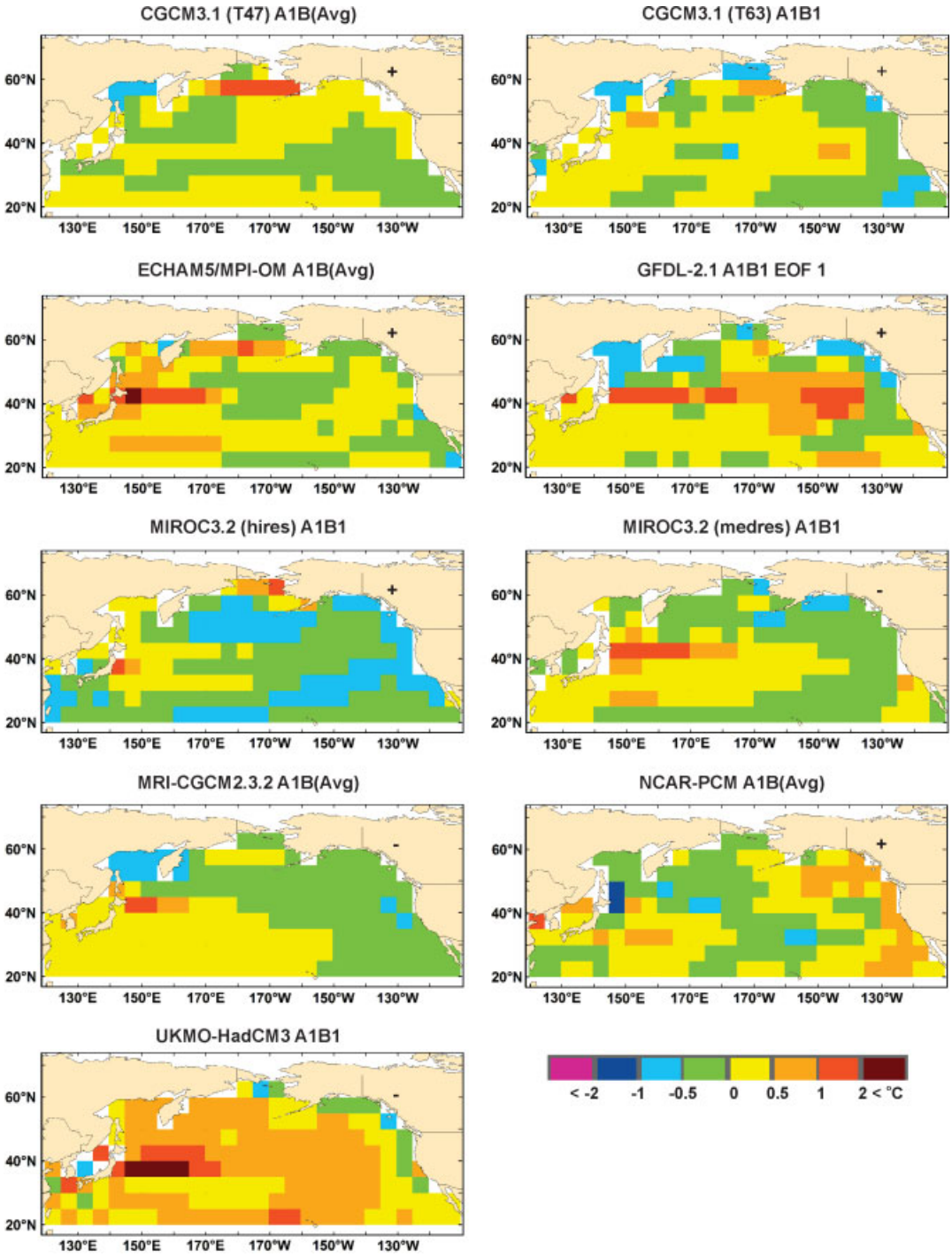

Figure 9. Plots of the differences between North Pacific SST residuals (°C) for 1950–1959 *versus* 2040–2049 for the A1B emissions scenario for each GCM. As a look-up aid, the plus or minus sign over the Yukon Territory, Canada, denotes whether a particular GCM run or average run showed a positive PDO shift (+) or negative PDO shift (−) in the 21st century as in Table III. This figure is available in colour online at wileyonlinelibrary.com/journal/joc

et al., 2001; Stahl *et al*., 2006). We presume that the same mechanism will continue to operate in some fashion in the early 21st century under global warming, as it did in the 20th century during the early stage of anthropogenic-forced increases in surface air temperatures and SSTs (Kaplan *et al*., 2000). As support for this hypothesis, all ten of the GCMs used in this study showed that the observed PDO is still present in the same form as the projected 2000–2050 North Pacific (Figures 5–7). Hence, it is reasonable to project the PDO by projecting the 2000–2050 residual SST anomalies from each of the GCMs onto the leading eigenvector from the 1900–1993 simulated GCM data. However, it seems uncertain to assume that this mechanism will operate as before when the global warming trend surpasses the natural North Pacific variability (Overland and Wang, 2007; Wang *et al*., 2010). These projections are not forecasts *sensu stricto* as the AR4 simulations evaluated here can be

considered to have random ocean initializations, whereas upper ocean heat content is a key component of any initialized forecast.

This study examines the concurrent projection of three atmosphere-ocean oscillations: the PDO, SOI and the NAO, rather than the typical one or two (Fyfe *et al*., 1999; Collins *et al*., 2005, 2010; van Oldenborgh *et al*., 2005; Yamaguchi and Noda, 2006; Meehl and Tang, 2007) and can therefore examine the relationships among them. First, interactions between the PDO and ENSO are discussed, then interactions between the PDO and the NAO.

The most recent consensus concerning the future status of ENSO is that the CMIP3 models project a more 'El Niño-like' mean state change, with no consistent indication of detectable future changes in ENSO amplitude, frequency or spatial pattern (Yamaguchi and Noda, 2006; IPCC4, 2007, Figure 10.16; Collins *et al*., 2005, 2010). This study's multi-model mean decrease in the SOI and typical responses of individual GCM runs are consistent with this consensus (Tables II and III). A shift of the characteristic ENSO spectral bands towards higher frequencies has been observed in GCM-derived ENSO spectra (van Oldenborgh *et al*., 2005), which is similar to this study's result of the characteristic PDO spectral bands shifting towards higher frequencies. Whether or not the PDO is independent of ENSO is uncertain, but an active area of research. Some researchers (Newman *et al*., 2003; Schneider and Cornuelle, 2005; Newman, 2007) have argued that ENSO drives the PDO, i.e. that El Niño (La Niña) drives the positive (negative) phase of the PDO. If this hypothesis is true, then as there will be more El Niño-like mean state conditions under global warming, then possibly more positive phase PDO-like conditions could result, depending on the exact nature of the driving mechanism. However, if the driving mechanism is a function of the base ENSO state, this does not accord with this study's projections, as 64% of the runs across all scenarios showed out-of-phase concurrent shifts between the SOI and the PDO, i.e. 64% of the runs showed a 2000–2050 mean shift towards a concurrent negative SOI (El Niño) and negative PDO, or positive SOI (La Niña) and positive PDO (Table III). On the other hand, other researchers (Zhang *et al*., 1996; Yu *et al*., 2007) have considered the PDO to be independent of ENSO, but that reinforcing interactions could occur between the two oscillations. Gershunov and Barnett (1998), Yu *et al*. (2007) and Wise (2010) found that there occurred an enhanced response of the Pacific-North American mode (Wallace and Gutzler, 1981) when the PDO and ENSO were in the same phase, i.e. when the PDO was in a negative phase and a La Niña occurred, the Pacific Northwest experienced cooler and wetter conditions, and the American southwest and northern Mexico experienced even warmer and drier conditions than normal in a negative PDO alone.

This study's result of a shift towards a more positive NAO, significant for the A1B and A2 emission scenarios, is in accord with the literature reviewed in the IPCC AR4 (2007) projecting a more positive AO. The projection of a more positive AO is consistent with a projection of a negative PDO shift, as a more positive AO suggests a weaker Aleutian Low which is more consistent with the negative phase of the PDO (Gershunov and Barnett, 1998). However, the individual GCM runs showed no consistent pattern of an in-phase relationship between the AO/NAO and the PDO (i.e. the PDO shifting negative and the NAO shifting positive or vice versa) (Table III). Yamaguchi and Noda (2006) examined CMIP2 GCMs for their ability to concurrently project the ENSO and the AO. They found that the GCMs projected a strong shift towards a positive AO and a weak El Niño or strong La Niña, or shifts towards a weak positive AO and a strong El Niño, but no shifts towards both a strong AO and a strong El Niño simultaneously. They observed that this was because of a more positive AO producing a weaker Aleutian Low, which is more consistent with La Niña. All ten CMIP3 GCMs considered here were chosen for their ability to simulate the PDO well. A more careful examination of these ten models' ability to simulate the AO might show that the GCMs best at simulating the AO are those producing results compatible with the concurrent PDO projection. In particular, the AO might be more accurately projected by a higher geopotential height and/or PCA method (Stoner *et al*., 2009), rather than our use of a two-point SLP difference method based on the NAO.

In conclusion, this study projects a weak mean North Pacific Ocean shift towards more negative PDO-like conditions for the early half of the 21st century, based on archived CMIP3 runs. However, the GCMs split between those showing a shift, often significant, towards more negative PDO-like conditions for all three scenarios, and those showing a contrary shift, also often significant, towards more positive PDO-like conditions for all runs and all three scenarios. It will be interesting to see if corresponding results from a similar analysis of data from the ongoing AR5 (CMIP5) climate prediction experiments will show more consistency. As well, research on the actual physical mechanisms producing the statistical PDO pattern will provide important insights for any future projections of North Pacific SST variability.

Acknowledgements

We acknowledge the international modelling groups for providing their data for analysis, the PCMDI for collecting and archiving the model data, the WCRP/CLIVAR Working Group on Coupled Models (WGCM), their CMIP and Climate Simulation Panels for organizing the model data analysis activity, and the IPCC WG1 TSU for technical support. We thank N. J. Mantua and Dennis Hartmann for their help with PDO computational details and B. R. Bonsal and two anonymous reviewers for their extremely helpful comments that greatly improved this manuscript. This research was funded by the Natural

Sciences and Engineering Research Council of Canada and Alberta Environment.

References

Anderson PJ, Piatt JF. 1999. Community reorganization in the Gulf of Alaska following ocean climate regime shift. *Marine Ecology Progress Series* **189**: 117–123.

Bjornsson H, Venegas SA. 1997. A manual for EOF and SVD analyses of climatic data. Technical Report 97-1, Department of Atmospheric and Oceanic Sciences and Centre for Climate and Global Change Research: McGill University. Montreal, Quebec.

Bond NA, Harrison DE. 2000. The Pacific Decadal Oscillation, air-sea interaction and central north Pacific winter atmospheric regimes. *Geophysical Research Letters* **27**: 731–734.

Bond NA, Overland JE, Spillane M, Stabeno P. 2003. Recent shifts in the state of the North Pacific. *Geophysical Research Letters* **30**: 2183. DOI: 10.1029/2003GL018597.

Bonsal BR, Shabbar A, Higuchi K. 2001. Impact of low frequency variability modes on Canadian winter temperature. *International Journal of Climatology* **21**: 95–108.

Chao Y, Ghil M, McWilliams JC. 2000. Pacific interdecadal variability in this century's sea surface temperatures. *Geophysical Research Letters* **27**: 2261–2264.

Chen D, Hare SR. 2006. Neural network and fuzzy logic models for Pacific halibut recruitment analysis. *Ecological Modelling* **195**: 11–19.

Collins M, CMIP Modelling Groups. 2005. El Niño- or La Niña-like climate change? *Climate Dynamics* **24**: 89–104.

Collins M, An SI, Cai W, Ganachaud A, Guilyardi E, Jin FF, Jochum M, Lengaigne M, Power S, Timmermann A, Vecchi G, Wittenberg A. 2010. The impact of global warming on the tropical Pacific Ocean and El Niño. *Nature Geoscience* **3**: 391–397. DOI: 10.1038/NGEO868.

Collins WD, Bitz CM, Blackmon ML, Bonan GB, Bretherton CS, Carton JA, Chang P, Doney SC, Hack JJ, Henderson TB, Kiehl JT, Large WG, McKenna DS, Santer BD, Smith RD. The Community Climate System Model Version 3 (CCSM3). *Journal of Climate* **19**: 2122–2143.

Davis RE. 1976. Predictability of sea surface temperature and sea level pressure anomalies over the North Pacific Ocean. *Journal of Physical Oceanography* **6**: 249–266.

Delworth TL, Rosati A, Stouffer RJ, Dixon KW, Dunne J, Findell K, Ginoux P, Gnanadesikan A, Gordon CT, Griffies SM, Gudgel R, Harrison MJ, Held IM, Hemler RS, Horowitz LW, Klein SA, Knutson TR, Lin S-J, Milly PCD, Ramaswamy V, Schwarzkopf MD, Sirutis JJ, Stern WF, Spelman MJ, Winton M, Wittenberg AT, Wyman B. 2006. GDFL's CM2 global coupled climate models. Part I: formulation and simulation characteristics. *Journal of Climate* **19**: 643–674.

Deser C, Phillips AS, Hurrell JW. 2004. Pacific interdecadal climate variability: linkages between the tropics and the North Pacific during boreal winter since 1900. *Journal of Climate* **17**: 3109–3124.

Di Lorenzo E, Schneider N, Cobb KM, Franks PJS, Chhak K, Miller AJ, McWilliams JC, Borgard SJ, Arango H, Curchitser E, Powell TM, Reviere P. 2008. North Pacific Gyre Oscillation links ocean climate and ecosystem change. *Geophysical Research Letters* **35**: L08607, DOI: 10.1029/2007GL032838.

Dima M, Lohmann G. 2007. A hemispheric mechanism for the Atlantic Multidecadal Oscillation. *Journal of Climate* **20**: 2706–2719.

Flato GM. 2005. *The Third Generation Coupled Global Climate Model (CGCM3)*. Available at http://www.cccma.bc.ec.gc.ca/models/cgcm3.shtml. Accessed January 2010.

Folland CK, Parker DE. 1990. Observed variations of sea surface temperature. In *Climate-Ocean Interaction*, Schlesinger ME (ed). Kluwer: Dordrecht, 21–52.

Folland CK, Parker DE. 1995. Correction of instrumental biases in historical sea surface temperature data. *Quarterly Journal of the Royal Meteorological Society* **121**: 319–367.

Francis RC, Hare SR, Hollowed AB, Wooster WS. 1998. Effects of interdecadal climate variability on the oceanic ecosystems of the NE Pacific. *Fisheries and Oceanography* **7**: 1–21.

Fyfe JC, Boer GJ, Flato GM. 1999. The Arctic and Antarctic Oscillations and their projected changes under global warming. *Geophysical Research Letters* **26**: 1601–1604.

Gershunov A, Barnett TP. 1998. Interdecadal modulation of ENSO teleconnections. *Bulletin of the American Meteorological Society* **79**: 2715–2725.

Gordon C, Cooper C, Senior CA, Banks HT, Gregory JM, Johns TC, Mitchell JFB, Wood RA. 2000. The simulation of SST, sea ice extents and ocean heat transports in a version of the Hadley Centre coupled model without flux adjustments. *Climate Dynamics* **16**: 147–168.

Hasumi H, Emori S. 2004. K-1 coupled GCM (MIROC) description. K-1 Technical Report 1, Center for Climate System Research: University of Tokyo. 39. Available at http://www.ccsr.u-tokyo.ac.jp/kyosei/hasumi/MIROC/tech-repo.pdf. Accessed February 2010.

IPCC4. 2007. Climate change 2007: the physical science basis. In *Contribution of Working Group I to the Fourth Assessment Report of the Intergovernmental Panel on Climate Change*, Solomon S, Qin D, Manning M, Chen Z, Marquis M, Avery KB, Tignor M, Miller HL (eds). Cambridge University Press: Cambridge.

Jones PD, Jonsson T, Wheeler D. 1997. Extension to the North Atlantic Oscillation using early instrumental pressure observations from Gibraltar and South-west Iceland. *International Journal of Climatology* **17**: 1433–1450.

Kaplan A, Kushnir Y, Cane MA. 2000. Reduced space optimal interpolation of historical marine sea level pressure: 1854–1992. *Journal of Climate* **13**: 2987–3002.

Kiem AS, Franks SW, Kuczera G. 2003. Multi-decadal variability of flood risk. *Geophysical Research Letters* **30**: 1035–1039.

Knutti R, Abramowitz G, Collins M, Eyring V, Gleckler PJ, Hewitson B, Mearns L. 2010. Good practice guidance paper on assessing and combining multi model climate projections.. In *Meeting Report of the Intergovernmental Panel on Climate Change Expert Meeting on Assessing and Combining Multi Model Climate Projections*, Stocker TF, Qin D, Plattner G-K, Tignor M, Midgley PM (eds). IPCC Working Group I Technical Support Unit, University of Bern: Bern.

Kushnir Y, Robinson WA, Bladé I, Hall NMJ, Peng S, Sutton R. 2002. Atmospheric GCM response to extratropical SST anomalies: synthesis and evaluation. *Journal of Climate* **15**: 2233–2256.

Lau NC. 1997. Interactions between global SST anomalies and the midlatitude atmospheric circulation. *Bulletin of the American Meteorological Society* **78**: 21–33.

Manly BFJ. 1998. *Randomization, Bootstrap and Monte Carlo Methods in Biology*, 2nd edn.. Chapman and Hall: London.

Mann ME, Lees JM. 1996. Robust estimation of background noise and signal detection in climatic time series. *Climatic Change* **33**: 409–445.

Mantua NJ, Hare SR. 2002. The Pacific Decadal Oscillation. *Journal of Oceanography* **58**: 35–44.

Mantua NJ, Hare SR, Zhang Y, Wallace JM, Francis RC. 1997. A Pacific interdecadal climate oscillation with impacts on salmon production. *Bulletin of the American Meteorological Society* **78**: 1069–1079.

McCabe GJ, Dettinger MJ. 2002. Primary modes and predictability of year-to-year snowpack variations in the western United States from teleconnections with Pacific Ocean climate. *Journal of Hydrometeorology* **3**: 13–25.

McCabe GJ, Betancourt JL, Gray ST, Palecki MA, Hidalgo HG. 2008. Associations of multi-decadla sea-surface temperature variability with US drought. *Quaternary International* **188**: 31–40.

McGowan JA, Cayan DR, Dorman LM. 1998. Climate-ocean variability and ecosystem response in the Northeast Pacific. *Science* **281**: 210–217.

Meehl GA, Tang H. 2007. Multi-model changes in El Niño teleconnections over North America in a future warmer climate. *Climate Dynamics* **29**: 779–790.

Meehl GA, Covey C, Delworth T, Latif M, McAvaney B, Mitchell JFB, Stouffer RJ, Taylor KE. 2007. The WCRP CMIP3 multimodel dataset, a new era in climate change research. *Bulletin of the American Meteorological Society* **88**: 1383–1394.

Minobe S. 1997. A 50–70 year climatic oscillation over the North Pacific and North America. *Geophysical Research Letters* **24**: 683–686.

Minobe S. 1999. Resonance in bidecadal and pentadecadal climate oscillations over the North Pacific: role in climatic regime shifts. *Geophysical Research Letters* **26**: 855–858.

Minobe S, Kuwano-Yoshida A, Komori N, Xie SP, Small RJ. 2008. Influence of the Gulf Stream on the troposphere. *Nature* **452**: 206–209.

Muller WA, Roeckner E. 2006. ENSO impact on midlatitude circulation patterns in future climate change projections. *Geophysical Research Letters* **33**: L05711. DOI: 10.1029/2005GL025032.

Nakicenovic NJ, Alcamo J, Davis G, de Vries B, Fenhann J, Gaffin S, Gregory K, Grübler A, Jung TY, Kram T, La Rovere EL,

Michaelis L, Mori S, Morita T, Pepper W, Pitcher H, Price L, Riahi K, Roehrl A, Rogner H-H, Sankovski A, Schlesinger M, Shukla P, Smith S, Swart R, van Rooijen S, Victor N, Dadi Z. 2000. *IPCC Special Report on Emissions Scenarios.* Cambridge University Press: Cambridge and New York.

Newman M. 2007. Interannual to decadal predictability of tropical and North Pacific sea surface temperatures. *Journal of Climate* **20**: 2333–2356.

Newman M, Compo GP, Alexander MA. 2003. ENSO-forced variability of the Pacific Decadal Oscillation. *Journal of Climate* **16**: 3853–3857.

Oshima K, Tanimoto Y. 2009. An evaluation of reproducibility of the Pacific Decadal Oscillation in the CMIP3 simulations. *Journal of the Meteorological Society of Japan* **87**: 755–770.

Overland JE, Wang M. 2007. Future climate of the North Pacific ocean. *EOS* **88**: 178.

Overland JE, Rodionov S, Minobe S, Bond N. 2008. North Pacific regime shifts: definitions, issues and recent transitions. *Progress in Oceanography* **77**: 92–102.

Overland JE, Alheit J, Bakun A, Hurrell JW, Mackas DL, Miller AJ. 2010. Climate controls on marine ecosystems and fish populations. *Journal of Marine Systems* **79**: 305–315.

Pavia EG, Graef F, Reyes J. 2006. PDO-ENSO effects in the climate of Mexico. *Journal of Climate* **19**: 6433–6438.

Pope VD, Gallani ML, Rowntree PR, Stratton RA. 2000. The impact of new physical parametrizations in the Hadley Centre climate model: HadAM3. *Climate Dynamics* **16**: 123–146.

Rayner NA, Parker DE, Horton EB, Folland CK, Alexander LV, Rowell DP, Kent EC, Kaplan A. 2003. Globally complete analyses of sea surface temperature, sea ice and night marine air temperature, 1871–2000. *Journal of Geophysical Research* **108**: 4407, DOI 10.1029/2002JD002670.

R Development Core Team. 2008. *R: A Language and Environment for Statistical Computing.* R Foundation for Statistical Computing: Vienna, Version 2.9.1. ISBN 3-900051-07-0. Available at http://www.R-project.org.

Redmond KT, Koch RW. 1991. Surface climate and streamflow variability in the western United States and their relationship to large-scale circulation indices. *Water Resources Research* **9**: 2381–2399.

Reynolds RW, Smith TM. 1995. A high-resolution global sea surface temperature climatology. *Journal of Climate* **8**: 1571–1583.

Rodionov SN, Bond NA, Overland JE. 2007. The Aleutian Low, storm tracks, and winter climate variability in the Bering Sea. *Deep-Sea Research II* **54**: 2560–2577.

Roeckner E, Bäuml G, Bonaventura L, Brokopf R, Esch M, Giorgetta M, Hagemann S, Kirchner I, Kornblueh L, Manzini E, Rhodin A, Schlese U, Schulzweida U, Tompkins A. 2003. The atmospheric general circulation model ECHAM5. Part I: Model description. Max-Planck-Institute for Meteorology Report, 127. Report No. 349. Available at http://edoc.mpg.de/175329. Accessed February 2010.

Ropelewski CF, Jones PD. 1987. An extension of the Tahiti-Darwin Southern Oscillation Index. *Monthly Weather Review* **115**: 2161–2165.

Schneider N, Cornuelle BD. 2005. The forcing of the Pacific Decadal Oscillation. *Journal of Climate* **18**: 4355–4373.

Stahl K, Moore RD, McKendry IG. 2006. The role of synoptic-scale circulation in the linkage between large-scale ocean-atmosphere indices and winter surface climate in British Columbia, Canada. *International Journal of Climatology* **26**: 541–560.

Stewart I, Cayan DR, Dettinger MD. 2005. Changes toward earlier streamflow timing across western North America. *Journal of Climate* **18**: 1136–1155.

St. Jacques JM, Sauchyn DJ, Zhao Y. 2010. Northern Rocky Mountain streamflow records: global warming trends, human impacts or natural variability? *Geophysical Research Letters* **37**: L06407, DOI: 10.1029/2009GL042045.

Stoner AMK, Hayhoe K, Wuebbles DJ. 2009. Assessing general circulation model simulations of atmospheric teleconnection patterns. *Journal of Climate* **22**: 4348–4372.

Trenberth KE, Hurrell JW. 1994. Decadal atmosphere-ocean variations in the Pacific. *Climate Dynamics* **9**: 303–319.

van Oldenborgh G, Philip S, Collins M. 2005. El Niño in a changing climate: a multi-model study. *Ocean Science* **1**: 81–95.

Verdon DC, Franks SW. 2006. Long-term behavior of ENSO: interactions with the PDO over the past 400 years inferred from paleoclimate records. *Geophysical Research Letters* **33**: L06712.

Wallace JM, Gutzler DS. 1981. Teleconnections in the geopotential height field during the Northern Hemisphere winter. *Monthly Weather Review* **109**: 784–812.

Wang M, Overland JE, Bond NA. 2010. Climate projections for selected large marine ecosystems. *Journal of Marine Systems* **79**: 258–266.

Washington WM, Weatherly JW, Meehl GA, Semtner AJ Jr, Bettge TW, Craig AP, Strand WG Jr, Arblaster J, Wayland VB, James R, Zhang Y. 2000. Parallel Climate Model (PCM) control and transient simulations. *Climate Dynamics* **16**: 755–774.

Whitfield PH, Moore RD, Fleming SW, Zawadzki A. 2010. Pacific Decadal Oscillation and the hydroclimatology of Western Canada – reviews and prospects. *Canadian Water Resources Journal* **35**: 1–28.

Wilks DS. 2006. *Statistical Methods in the Atmospheric Sciences*, 2nd edn. Academic Press: New York.

Wise EK. 2010. Spatiotemporal variability of the precipitation dipole transition zone in the western United States. *Geophysical Research Letters* **37**: L07706.

Yamaguchi K, Noda A. 2006. Global warming patterns over the North Pacific: ENSO versus AO. *Journal of the Meteorological Society of Japan* **84**: 221–241.

Yu B, Zwiers FW. 2007. The impact of combined ENSO and PDO on the PNA climate: a 1,000-year climate modeling study. *Climate Dynamics* **29**: 837–851.

Yu B, Shabbar A, Zwiers FW. 2007. The enhanced PNA-like climate response to Pacific interannual and decadal variability. *Journal of Climate* **20**: 5285–5300.

Yukimoto S, Noda A. 2003. Improvements of the Meteorological Research Institute Global Ocean-Atmosphere Coupled GCM (MRI-GCM2) and its climate sensitivity. In *CGER's Supercomputing Activity Report*, Fujinuma Y, Miyamoto N, Tanaka K, Kaizu H (eds). Vol. 10–2001. National Institute for Environmental Studies: Ibaraki, 37–44.

Yukimoto S, Noda A, Kitoh A, Sugi M, Kitamura Y, Hosaka M, Shibata K, Maeda S, Uchiyama T. 2001. The new Meteorological Research Institute global ocean-atmosphere coupled GCM (MRICGCM2)–Model climate and variability. *Papers in Meteorology and Geophysics* **51**: 47–88.

Zhang Y, Wallace JM, Iwasaka N. 1996. Is climate variability over the North Pacific a linear response to ENSO? *Journal of Climate* **9**: 1468–1478.

Zhang Y, Wallace JM, Battisti DS. 1997. ENSO-like interdecadal variability: 1900–1993. *Journal of Climate* **10**: 1004–1020.

Zhang C, Lee JB, Seo Y, Yoon SC, Kim S. 2004. Variations in the abundance of fisheries resources and ecosystem structure in the Japan/East Sea. *Progress in Oceanography* **61**: 245–265.

